

1
2
3
4
5
6
7
8
9
10
11
12
13
14
15
16
17
18

Comparison of single genome and allele frequency data reveals discordant demographic histories

Annabel C. Beichman^{*}, Tanya N. Phung[†], and Kirk E. Lohmueller^{*,†,‡}

Affiliations:

^{*}Department of Ecology and Evolutionary Biology, University of California, Los Angeles, CA 90095, USA.

[†]Interdepartmental Program in Bioinformatics, University of California, Los Angeles, CA 90095, USA.

^{*,†,‡}Department of Human Genetics, David Geffen School of Medicine, University of California, Los Angeles, CA 90095, USA.

19 **Short title:** Disparate demographic histories

20

21

22 **Keywords:** Pairwise Sequentially Markovian Coalescent, site frequency spectrum, population
23 genetics, demographic inference, non-model organisms

24

25

26

27 **To whom correspondence should be addressed:**

28 Kirk E. Lohmueller

29 Department of Ecology and Evolutionary Biology

30 University of California, Los Angeles

31 621 Charles E. Young Drive South

32 Los Angeles, CA 90095-1606

33 (310)-825-7636

34 klohmueller@ucla.edu

35

36

37

38

39

40

41

42

43

44

45

46

47

48 **ABSTRACT.** Inference of demographic history from genetic data is a primary goal of
49 population genetics of model and non-model organisms. Whole genome-based approaches such
50 as the Pairwise/Multiple Sequentially Markovian Coalescent (PSMC/MSMC) methods use
51 genomic data from one to four individuals to infer the demographic history of an entire
52 population, while site frequency spectrum (SFS)-based methods use the distribution of allele
53 frequencies in a sample to reconstruct the same historical events. Although both methods are
54 extensively used in empirical studies and perform well on data simulated under simple models,
55 there have been only limited comparisons of them in more complex and realistic settings. Here
56 we use published demographic models based on data from three human populations (Yoruba
57 (YRI), descendants of northwest-Europeans (CEU), and Han Chinese (CHB)) as an empirical
58 test case to study the behavior of both inference procedures. We find that several of the
59 demographic histories inferred by the whole genome-based methods do not predict the genome-
60 wide distribution of heterozygosity nor do they predict the empirical SFS. However, using
61 simulated data, we also find that the whole genome methods can reconstruct the complex
62 demographic models inferred by SFS-based methods, suggesting that the discordant patterns of
63 genetic variation are not attributable to a lack of statistical power, but may reflect unmodeled
64 complexities in the underlying demography. More generally, our findings indicate that
65 demographic inference from a small number of genomes, routine in genomic studies of non-
66 model organisms, should be interpreted cautiously, as these models cannot recapitulate other
67 summaries of the data.

68

69

INTRODUCTION

70

71 The Pairwise Sequentially Markovian Coalescent (PSMC) and related methods have
72 become a popular tool to estimate the history of a population from genetic variation data
73 (McVean and Cardin 2005; Li and Durbin 2011; Schiffels and Durbin 2014). These methods use
74 whole genome sequences from one to four individuals to infer the demographic history of an
75 entire population. Specifically, they estimate the local time to the most recent common ancestor
76 (TMRCA) for small regions in the genome, then use the distribution of these coalescent times to
77 infer an overarching demographic history. For instance, if many regions of the genome coalesce
78 at a specific time, it may be evidence for a population contraction, which would reduce the
79 number of genetic lineages. The great appeal of these methods is that they do not rely on deep
80 sequencing of multiple individuals in a population; instead, a single genome can be used to infer
81 the demographic history of an entire population. PSMC and its successors have been used to
82 infer the demographic histories and split times of many human populations (Li and Durbin 2011;
83 Kidd *et al.* 2012; Schiffels and Durbin 2014; 1000 Genomes Project Consortium 2015; Henn *et*
84 *al.* 2016), and were recently featured in three prominent articles that reconstructed human history
85 using whole genome sequencing data from over 20 populations (Malaspinas *et al.* 2016; Mallick
86 *et al.* 2016; Pagani *et al.* 2016).

87 PSMC plots have also become a cornerstone of many studies of non-model organisms
88 lacking resources for the sequencing of numerous individuals, including archaic hominins
89 (Meyer *et al.* 2012; Prufer *et al.* 2014), great apes (Prado-Martinez *et al.* 2013), wild boars and
90 domestic pigs (Groenen *et al.* 2012; Bosse *et al.* 2014), canids (Freedman *et al.* 2014; Wang *et*
91 *al.* 2016), horses (Orlando *et al.* 2013), over 38 bird species (Nadachowska-Brzyska *et al.* 2013;

92 Hung *et al.* 2014; Nadachowska-Brzyska *et al.* 2015; 2016; Murray *et al.* 2017), pandas (Zhao *et al.* 2012), dromedaries (Fitak *et al.* 2016), flowering plants (Albert *et al.* 2013; Ibarra-Laclette *et al.* 2013; Holliday *et al.* 2016), and even woolly mammoths (Palkopoulou *et al.* 2015).

95 Despite their wide-spread prominence, there is concern over the validity of demographic
96 models obtained from this set of whole genome-based methods. Particularly, Mazet *et al.* (2015)
97 found that PSMC captures the inverse instantaneous coalescent rate (IICR) rather than an
98 absolute measure of population size. The IICR corresponds to the effective population size if the
99 population is panmictic, but it can differ from the population size due to gene flow and
100 population structure which affect the time to coalescence between subgroups. Thus, population
101 structure can give a false signal of population growth or contraction – a notorious problem in
102 demographic inference (Ptak and Przeworski 2002; Chikhi *et al.* 2010; Peter *et al.* 2010;
103 Gattepaille *et al.* 2013; Heller *et al.* 2013; Mazet, Rodriguez, and Chikhi 2015; Mazet,
104 Rodriguez, Grusea, *et al.* 2015; Orozco-terWengel 2016). Given these possible confounders, the
105 degree to which whole genome-based plots derived from PSMC and its successors correspond to
106 actual population size changes, rather than other demographic phenomena, remains unclear.

107 An alternative approach to infer population demography from genetic data uses the site
108 frequency spectrum (SFS). The SFS represents the distribution of alleles at different frequencies
109 in a sample of individuals from a population (Nielsen 2000; Wakeley 2009). The distribution of
110 single nucleotide polymorphisms (SNPs), ranging from rare ‘singletons’ which appear only once
111 in the sample, to high-frequency variants that may appear in the majority of individuals, is
112 directly affected by the demographic history of the population (Nielsen 2000; Wakeley 2009).
113 Population contractions (‘bottlenecks’) can lead to a dearth of rare variants (Nei *et al.* 1975),

114 whereas a rapid population expansion can lead to an overabundance (Tajima 1989; Slatkin and
115 Hudson 1991; Keinan and Clark 2012). The SFS is a sufficient statistic for unlinked SNPs and
116 has been used extensively in population genetic inference of demography (Nielsen 2000;
117 Polanski and Kimmel 2003; Adams and Hudson 2004; Marth *et al.* 2004; Keinan *et al.* 2007;
118 Gutenkunst *et al.* 2009; Gravel *et al.* 2011; Excoffier *et al.* 2013). SFS-based demographic
119 inference has been implemented in programs such as $\partial a \partial i$ (Gutenkunst *et al.* 2009), moments
120 (Jouganous *et al.* 2017), fastsimcoal2 (Excoffier *et al.* 2013), stairway plot (Liu and Fu 2015),
121 fastNeutrino (Bhaskar *et al.* 2015), and others (Schraiber and Akey 2015). The SFS requires less
122 sequence data per individual than the whole genome methods, but requires a greater number of
123 individuals to be studied, with a minimum of ten per population typically used (Gutenkunst *et al.*
124 2009; Excoffier *et al.* 2013). While the SFS is impractical if one can only sequence one or two
125 individuals per population, population genomic studies based on many short loci scattered
126 throughout the genome are beginning to be carried out on non-model organisms. RAD-seq data
127 or gene transcript data from RNA-seq can readily be used for SFS-based demographic inference
128 (McCoy *et al.* 2014; Trucchi *et al.* 2014; Sovic *et al.* 2016).

129 SFS-based and whole genome-based methods may have different strengths and
130 weaknesses for demographic inference (Schraiber and Akey 2015). Theoretical and empirical
131 data show that SFS-based approaches using large numbers of individuals can accurately estimate
132 recent population growth (Nelson *et al.* 2012; Tennessen *et al.* 2012; Gazave *et al.* 2013;
133 Bhaskar *et al.* 2015; Gao and Keinan 2016). In contrast, whole genome-based methods are less
134 able to do so (Li and Durbin 2011). Recently, however, Schiffels and Durbin (2014) developed
135 the multiple sequentially Markovian coalescent (MSMC), an extension to PSMC that uses the

136 SMC' algorithm (Marjoram and Wall 2006) and can infer demography from two, four or eight
137 haplotypes (also known as PSMC' when inferring from two haplotypes). The incorporation of
138 multiple genomes in MSMC is specifically meant to improve estimates of recent growth
139 (Schiffels and Durbin 2014).

140 The SFS may be limited in the degree to which it can detect ancient bottlenecks $> 2N_e$
141 (effective population size) generations ago and in its ability to detect population declines
142 (Bunnefeld *et al.* 2015; Terhorst and Song 2015; Boitard *et al.* 2016). Whole genome-based
143 approaches are not constrained *a priori* by the number of population size changes as is common
144 in the SFS-based approaches (but see the “stairway plot” approach of Liu and Fu (2015)). They
145 therefore often give information about events occurring millions of years ago, but the reliability
146 of those results remains uncertain (Li and Durbin 2011). Further, demographic models inferred
147 from human populations using the SFS were unable to recapitulate the empirical distribution of
148 identity by state (IBS) tracts across the genome, while PSMC-derived models and a new IBS-
149 derived model were better able to match the IBS tract distribution (Harris and Nielsen 2013).
150 However, the IBS-derived model did not predict the empirical SFS.

151 Due to these different strengths and weaknesses of approaches using a single type of data,
152 new methods have been developed which attempt to combine linkage disequilibrium (LD)
153 information and the SFS (Bunnefeld *et al.* 2015; Boitard *et al.* 2016; Terhorst *et al.* 2017;
154 Weissman and Hallatschek 2017). One of the most recent is Terhorst, Kamm and Song’s (2017)
155 method, SMC++, which combines a PSMC-like approach with the SFS to condition an SFS
156 calculated from many individuals on the distribution of TMRCA from a single unphased
157 genome. This approach is fast and potentially very powerful, but has the same barrier to entry for

158 those studying non-model organisms as the other SFS methods, as it requires sequence data from
159 many individuals.

160 Due to anthropological and biomedical interest, humans are an organism that has been
161 extensively studied using numerous demographic inference methods and provide a means to
162 quantitatively compare these demographic inference approaches using the same empirical
163 populations. Gutenkunst *et al.* (2009) and Gravel *et al.* (2011) carried out SFS-based inference of
164 human demography using the diffusion approximation in $\partial a \partial i$, while Li and Durbin (2011) and
165 Schiffels and Durbin (2014) estimated human demography from the same populations using
166 PSMC and MSMC, respectively. Although the results are in some ways generally similar, the
167 demographic models inferred for three human populations using MSMC (Schiffels and Durbin
168 2014) differ from demographic models for the same populations derived from SFS-based
169 methods (Gutenkunst *et al.* 2009). MSMC infers ancient ancestral sizes and periods of growth
170 and decline (the characteristic “humps” in MSMC trajectories) that were not detected in the SFS-
171 derived models as well as inferring greater recent growth (**Figure 1**). The models inferred using
172 MSMC also vary depending on the number of genomes used for the inference (**Figure 1**).

173 Terhorst *et al.* (2017) analyzed the same populations with the combined whole genome
174 and SFS method, SMC++, finding an ancestral size more in line with Gutenkunst *et al.*'s (2009)
175 model, but with greater recent growth and ancestral bottlenecks more resembling the MSMC
176 models (**Figure 1**). The reasons why these approaches to demographic inference yield different
177 estimates remain poorly understood.

178 Here we leverage humans as a model system to perform an empirical comparison of the
179 performance of whole genome, SFS, and combined methods of demographic inference.

180 Specifically, we determine which published models of human demography described above
181 (**Figure 1**) best fit the empirical distributions of genome-wide heterozygosity, LD decay, and the
182 observed SFS.

183 We find that the models inferred using the SFS or the combined method SMC++
184 accurately recapitulate heterozygosity and the observed SFS. Among the MSMC models inferred
185 by Schiffels and Durbin (2014), only the MSMC models based on a single genome were able to
186 accurately recapitulate heterozygosity, and none of the MSMC models predicted an SFS that
187 matched the empirical SFS. None of the demographic histories accurately predicted LD decay,
188 but the histories derived from MSMC using four genomes (8 haplotypes), the SFS, and SMC++
189 based models fit better than the MSMC models based on one or two genomes. Our results
190 provide a cautionary tale against the literal interpretation of demographic models inferred using
191 one type of data, instead arguing for considering multiple summaries of the data when making
192 detailed demographic inferences in non-model species.

193

194

METHODS

195 **Published demographic models used in this study**

196 We determined which, if any, of the published models of human demography (**Figure 1**)
197 described below could accurately predict multiple summaries of the genetic variation data.
198 Demographic models that fit the data well should produce patterns of genetic variation that
199 match the empirical patterns in the data. We focused on three human populations: Utah residents
200 with Northern and Western European ancestry from the Centre d'Etude du Polymorphisme

201 Humain (CEPH) collection (CEU), Han Chinese in Beijing, China (CHB), and Yoruba in Ibadan,
202 Nigeria (YRI).

203 The first set of demographic models was jointly inferred for the three populations in $\partial a \partial i$
204 by Gutenkunst *et al.* (2009) using a three-population joint SFS based on data from intronic
205 regions. Their model parameters were made available both in $\partial a \partial i$ and Hudson's ms (Hudson
206 2002) format, and include gene flow between the three populations (here referred to as the
207 "Gutenkunst" model).

208 The next nine models were inferred by Schiffels and Durbin (2014) using whole genome
209 Complete Genomics (Drmanac *et al.* 2010) sequence data of two, four and eight statistically
210 phased genomic haplotypes (1, 2 and 4 individual genomes) per population to infer demographic
211 histories using MSMC (here referred to as the "MSMC 2-Haplotype", "MSMC 4-Haplotype",
212 and "MSMC 8-Haplotype" models; **Supplementary Note 1**).

213 To analyze their models with $\partial a \partial i$, we converted these nine demographic models (CEU,
214 CHB, YRI populations, each based on two, four and eight haplotypes) into step-wise models of
215 population size changes over small time intervals (**Supplementary Note 2, Figure S1**).

216 The final set of models was inferred by Terhorst *et al.* (2017) in SMC++, a combined
217 SFS plus whole genome approach. For the whole genome portion of the analysis, they used high
218 coverage sequence data from Complete Genomics, and generated an SFS based on a combination
219 of 1000 Genomes and Complete Genomics whole genome data for each population (Drmanac *et al.*
220 *et al.* 2010; 1000 Genomes Project Consortium 2015; Terhorst *et al.* 2017). We converted these
221 SMC++ models to $\partial a \partial i$ and ms format in the same manner as the MSMC models (here referred
222 to as the "SMC++" models; **Supplementary Note 2**).

223 Heterozygosity predicted by demographic models

224 We compared the distribution of expected heterozygosity from data simulated under each
225 demographic model to empirical 1000 Genomes data from the same populations in order to
226 determine which models most accurately predict this broad summary of the data (**Figure 2;**
227 **Table S1**). While heterozygosity is a summary of the SFS, we considered it valuable to examine
228 both statistics since information regarding the spatial correlation among SNPs along the genome
229 is lost in the genome-wide SFS. The distribution of heterozygosity across windows of the
230 genome retains some spatial information and is more similar to what is used by the MSMC
231 inference approach.

232 *Empirical heterozygosity:* 1000 Genomes data from the CEU, CHB and YRI populations were
233 downloaded. Ten unrelated individuals per population (see **Supplementary Note 3** for sequence
234 IDs) were randomly chosen so that comparisons could be made with Gutenkunst *et al.*'s (2009)
235 empirical SFS, described below. For all our empirical analyses, only sites that passed the 1000
236 Genomes "Strict Mask" filter were considered (1000 Genomes Project Consortium 2015).

237 Expected heterozygosity per site (π) was calculated in non-overlapping 100kb windows
238 from the whole genome data (**Supplementary Note 3**) as:

$$239 \quad \pi = \frac{n}{n-1} \frac{\sum_{i=1}^L 2p_i(1-p_i)}{L}$$

240 where p is the frequency of one allele, L is the total number of callable sites in the window, and n
241 is number of sampled chromosomes ($n = 20$ for 10 diploid individuals).

242 Because genetic variation can be affected by linked natural selection (Gazave *et al.* 2014;
243 Schrider *et al.* 2016), we also calculated expected heterozygosity for a set of 6333 x 10kb neutral
244 windows that were selected using the Neutral Region Explorer (NRE) (Arbiza *et al.* 2012)

245 **(Supplementary Note 3; Figure S2)**. The NRE is a useful tool that allows for the quick
246 identification of putatively neutral regions that have high recombination rates and high B -values
247 (indicating less linked selection). For the full set of parameters used in selection of putatively
248 neutral regions, see **Supplementary Note 3**.

249 *Simulated heterozygosity*: For each demographic model, whole genome data for 10 individuals
250 were simulated in MaCS (Chen *et al.* 2009) over 20,000 x 100kb independent blocks, each with
251 a different recombination rate drawn from the distribution of recombination rates calculated by
252 Phung *et al.* (2016) from the pedigree-based genetic map assembled by the deCODE project
253 (Kong *et al.* 2010). Additionally, 6300 x 10kb independent blocks per 10 individuals were
254 simulated for comparison to the neutral regions from the 1000 Genomes dataset (1000 Genomes
255 Project Consortium 2015). Each 10kb block was simulated using a recombination rate matched
256 to that of one of the empirical neutral 10kb windows, linearly interpolated from the deCODE
257 project (Kong *et al.* 2010). For both sets of simulations, the expected heterozygosity across the
258 10 individuals was calculated using the equation above in msstats (Hudson 2002).

259

260 **Linkage disequilibrium decay predicted by demographic models**

261 We calculated LD between pairs of SNPs using genotype data from 10 individuals from
262 each of the four populations in the 1000 Genomes Project data. We removed singletons and sites
263 where all ten individuals were homozygous for the reference allele and then calculated genotype
264 r^2 using vcftools (Danecek *et al.* 2011). All pairs of SNPs were then placed into bins based on
265 their physical distance (bp) between each other, from 0-1000bp (bin 1) to 50,000-51,000bp (bin
266 51). Within each bin, the average r^2 was calculated by dividing the sum of r^2 values of each pair

267 of SNPs in the bin by the total number of SNP pairs in that bin.

268 The same procedure was carried out for the data simulated in MaCS (Chen *et al.* 2009)
269 that were used for the calculations of heterozygosity above. The MaCS output was converted to
270 vcf format using a custom bash script. Genotype r^2 was calculated in vcftools (Danecek *et al.*
271 2011) for each 100kb simulated window, the SNP pairs were binned by distance, and average r^2
272 was calculated as described above. The MSMC 8-Haplotype YRI and MSMC 4-Haplotype CEU,
273 CHB and YRI models have extremely large ancestral sizes, and so their simulations involve so
274 many SNPs that the LD calculations become highly computationally intensive. Therefore, for
275 these models only 5000 x 100kb blocks were used for LD decay calculations, with 20,000 x
276 100kb blocks used for the other models. We experimented with down-sampling the results and
277 found no change in the LD decay curve due to the smaller amount of data.

278 To demonstrate that the use of the SMC' approximation in the MaCS (Chen *et al.* 2009)
279 simulator was not biasing our estimates of LD, we simulated data in the manner described above
280 under a simple model of extreme population decline (from 100,000 ancestral individuals to 1000)
281 using both MaCS and MSMS (Ewing and Hermisson 2010) (which does not use the SMC'
282 approximation) and ran it through the same LD decay pipeline used for our other simulated data
283 (**Figure S3**).

284

285 **SFS predicted by demographic models**

286 We used the diffusion approximation in $\partial a \partial i$ (Gutenkunst *et al.* 2009) to calculate the
287 expected SFSs under the Gutenkunst, MSMC 2-Haplotype, MSMC 4-Haplotype, MSMC 8-
288 Haplotype, and SMC++ models for the CEU, CHB and YRI populations. We compared the SFSs

289 expected under each of these models both to the empirical SFS used by Gutenkunst *et al.* (2009)
290 to infer the demographic histories of these three populations (“Observed (Gutenkunst)”, **Figure**
291 **4-5**) as well as to the SFSs based on low-coverage 1000 Genomes whole genome sequencing
292 data (“1000 Genomes (Whole Genome)”, **Figure 6**) and SFSs based on putatively neutral
293 regions in the 1000 Genomes dataset (“1000 Genomes (Neutral)”, **Figure 6**). We assessed the fit
294 of different models to the observed SFS by comparing their log-likelihoods (see below,
295 **Supplementary Note 4; Table 1, S2-S4**).

296
297 *Empirical SFSs*: The primary empirical SFSs used in our comparisons were produced by
298 Gutenkunst *et al.* (2009) and used to infer the joint demographic histories of CEU, CHB and YRI
299 populations in their study (“Observed (Gutenkunst)”). As described in their supplementary
300 information, the joint SFS represents 4.04Mb of Sanger sequencing data from 12 YRI, 12 CHB
301 and 22 CEU individuals projected down to 20 chromosomes for a total of 17,446 segregating
302 SNPs polarized against chimp, with a correction for ancestral misidentification applied. We
303 marginalized the SFS using $\partial a \partial i$ (Gutenkunst *et al.* 2009), in order to have one SFS per
304 population (**Figure 4, 5**).

305 In order to make sure our results were consistent with SFSs derived from other
306 sequencing methodologies and different genomic regions, we also generated folded proportional
307 genome-wide and neutral SFSs from the 1000 Genomes data described above (“1000 Genomes
308 (WG)” and “1000 Genomes (Neutral)”) (1000 Genomes Project Consortium 2015)
309 (**Supplementary Note 3; Figure 6, S7**).

310 *Expected SFSs under published demographic models:* Expected SFSs for a sample size of 10
311 diploid individuals were calculated in $\partial a \partial i$ (2009) for each of the published demographic models
312 extrapolating calculations across three grid points (40, 50, 60) (**Figure 4, 5**). To test whether the
313 effect of differences in mutation rate between the studies may be responsible for discrepancies,
314 we also considered an alternative scaling of the MSMC models using a higher mutation rate
315 (**Supplementary Note 5**).

316 We generated both the proportional (**Figure 4, S5**) and absolute (i.e. SFS based on SNP
317 counts) SFSs (**Figure 5, S6**). The proportional SFS was calculated by dividing each bin of the
318 SFS output by $\partial a \partial i$ by the sum of the bins. The absolute SFS was calculated by scaling the SFS
319 output by $\partial a \partial i$ (which is relative to $\theta = 1$) by:

$$320 \theta = 4N_{Ai}\mu L$$

321 where N_{Ai} is the oldest ancestral size inferred in each model and L is the sequence length
322 (4.04Mbp), in Gutenkunst *et al.* (2009). θ for the Gutenkunst model used the authors' preferred
323 mutation rate, $\mu = 2.35 \times 10^{-8}$ mutations per base per generation, and θ for the MSMC and
324 SMC++ models used the authors' preferred mutation rate of $\mu = 1.25 \times 10^{-8}$ mutations per base per
325 generation (see **Supplementary Note 5** for scaling using alternate mutation rates).

326 *Assessing SFS fit:* Log-likelihoods were calculated for each proportional SFS relative to the each
327 of the three observed SFSs (Observed (Gutenkunst), 1000 Genomes (Whole Genome), and 1000
328 Genomes (Neutral)) using a multinomial log-likelihood (**Supplementary Note 4; Table 1, S2,**
329 **S4**). The fit of different models was compared by examining their decrease in log-likelihood
330 compared to that of each of the observed SFSs to itself (**Supplementary Note 4; Table 1, S2,**
331 **S4**). Due to the uncertainty of singleton SNP calls using high-throughput sequencing data, log-

332 likelihoods were calculated both with singletons and with the SFS renormalized without the
333 singletons category when comparing to the 1000 Genomes SFSs (**Figure S7; Table S4**).

334 Log-likelihoods were calculated for each absolute SFS (in terms of SNP counts) using a
335 Poisson likelihood relative to the Observed (Gutenkunst) SFS (**Supplementary Note 4; Table**
336 **S3**).

337 **Effect of Uncertainty in Ancestral Population Size**

338 To investigate whether changing the ancestral population size (N_A) in the MSMC trajectories
339 would result in SFSs that better fit the observed SFS, we adjusted the CEU MSMC 2-Haplotype
340 model to have a variety of N_A values. We also trimmed the model to remove ancient events
341 (older than 225.5 kya) to better match the time period (in years) encompassed by the Gutenkunst
342 *et al.*'s (2009) model. These adjusted stepwise models were then used to calculate the expected
343 SFS in $\partial a \partial i$, as above. **Supplementary Note 7** describes the values of N_A used when testing the
344 trimmed and untrimmed models (**Figure S10-S13**).

345

346 **MSMC Population Size Trajectories for Demographic Models Inferred from the SFS**

347 To determine whether MSMC is capable of inferring a demography as complex as the
348 one inferred in the Gutenkunst model, we used coalescent simulations to generate long
349 chromosomal sequence data for each population under the Gutenkunst *et al.* (2009) inferred
350 demographic model (see Gutenkunst *et al.*'s (2009) Figure 2B and Table 1 for full model), then
351 ran MSMC on these simulated datasets to assess whether the program is capable of recovering
352 the underlying demographic model.

353 Simulations were carried out using MaCS (Chen *et al.* 2009). For each population, we

354 simulated 50 replicate “genomes,” made up of 80 independent 30Mb “chromosomes,” each made
355 up of 300 linked 100kb recombination blocks, with per-block recombination rates calculated by
356 Phung *et al.* (2016) from the pedigree-based genetic map assembled by the deCODE project
357 (Kong *et al.* 2010).

358 Each simulated genome was then used for a separate MSMC inference, using the default
359 parameters (Schiffels and Durbin 2014) (**Figure 7A**). To determine whether these inferred
360 MSMC trajectories would lead to SFSs matching those predicted by Gutenkunst *et al.*'s (2009)
361 model, the MSMC trajectories were averaged and the average was converted into a step-wise
362 $\partial a \partial i$ model. This model was then used to calculate the expected SFS under the averaged model
363 based on simulated data (**Figure 7B-C**). The multinomial and Poisson log-likelihoods for the
364 proportional and SNP count SFSs were calculated as described in **Supplementary Note 4**
365 (**Table S2, S3**).

366 *Extreme Recent Growth and Neanderthal Admixture:* We simulated data under more complex
367 demographic histories, first to explore MSMC 2-Haplotype and 8-Haplotype's relative abilities
368 to infer extreme recent growth, then to determine whether the addition of Neanderthal admixture
369 may lead to MSMC trajectories resembling those inferred from real data by Schiffels and Durbin
370 (2014) (**Supplementary Note 6; Figure S8-S9**).

371

372 **Data Availability**

373 All code to simulate data under each demographic model and calculate heterozygosity and
374 generate the SFS from simulated and empirical data are available on GitHub:
375 github.com/LohmuellerLab/Compare_Demographic_Models

376

RESULTS

377 We compared published models of demography for three human populations (CEU,
378 CHB, YRI) inferred using different methods for demographic inference: (1) using the SFS in
379 $\partial a \partial i$ (“Gutenkunst”) (Gutenkunst *et al.* 2009); (2) using whole genomes in MSMC (“MSMC 2,
380 4, 8-Haplotype”) (Schiffels and Durbin 2014); (3) using a combined SFS plus whole genome
381 approach in SMC++ (“SMC++”) (Terhorst *et al.* 2017). The evaluation of the MSMC models
382 involves three models per population because Schiffels and Durbin’s (2014) inference was
383 carried out using 2, 4, or 8 chromosomal haplotypes (from one, two and four individuals),
384 sometimes resulting in fundamentally different demographic parameter estimates. We evaluated
385 whether the method’s performance was improved using certain numbers of haplotypes.

386

387 Heterozygosity predicted by demographic models

388 The distribution of expected heterozygosity across 100kb and 10kb blocks was calculated
389 from data simulated under each published demographic model for each of the three populations
390 and compared to empirical distributions of heterozygosity based on whole genome and putatively
391 neutral sequence data from the 1000 Genomes project.

392 We find that the Gutenkunst demographic model inferred from the SFS, the MSMC 2-
393 Haplotype model and the SMC++ model all yielded distributions of heterozygosity that resemble
394 the empirical whole genome distribution of heterozygosity, with MSMC 2-Haplotype fitting the
395 mean most closely (**Figure 2**). However, we found that the higher haplotype MSMC models
396 (MSMC 4-Haplotype and 8-Haplotype) yielded distributions of heterozygosity that were highly
397 divergent from the empirical distribution (**Figure 2; Table S1**).

398 The MSMC 4-Haplotype models fit worst due to their extremely high inferred ancestral
399 size across all three populations (**Figure 1; Table S2**; CEU: 187,514; CHB: 191,238; YRI:
400 205,845 individuals, compared to 4,000-40,000 individuals in the other models), with mean
401 whole genome heterozygosity distributions nearly 7x larger than that of the empirical whole
402 genome distribution (**Figure 2; Table S1**). The MSMC 8-Haplotype model for YRI infers a
403 similarly large ancestral size and has a similarly high mean heterozygosity to the 4-Haplotype
404 YRI model. The MSMC 8-Haplotype models for CEU and CHB, however, infer much lower
405 ancestral sizes (CEU: 2,147, CHB: 5,666) (**Figure 1**). Due to the low ancestral size, these models
406 also do not fit the empirical distribution well, yielding distributions of heterozygosity with means
407 that are 2-4x lower than the empirical distributions.

408 When examining the 1000 Genomes data, we found that heterozygosity in the neutral
409 regions was higher than that seen for the genome wide distribution of heterozygosity calculated
410 in 10kb windows (**Table S1**; e.g. CEU mean heterozygosity per site, whole genome: 7.8×10^{-4} vs.
411 neutral: 9.4×10^{-4}), suggesting that natural selection has directly and/or indirectly affected
412 genome-wide patterns of heterozygosity. When the published demographic models were
413 compared to the neutral heterozygosity distributions, we found similar trends to those seen for
414 the whole genome data (**Figure S2**).

415

416 **Linkage disequilibrium predicted by demographic models**

417 None of the published demographic models could perfectly recapitulate the empirical LD
418 decay curve (**Figure 3**). For SNP pairs less than 10kb apart, the MSMC-8 Haplotype model
419 comes closest to the empirical curve for the CEU and CHB populations (**Figures 3A and 3B**),

420 but underestimates the amount of LD, while all other models predict too much LD. The
421 Gutenkunst and SMC++ models predict similar LD curves and are closer to the empirical curve
422 than the MSMC 2-Haplotype and 4-Haplotype models. For YRI SNP pairs less than 10kb apart,
423 SMC++ and MSMC 8-Haplotype predict similar LD decay curves and are close to the empirical
424 distribution, with Gutenkunst still fitting better than MSMC 2-Haplotype and 4-Haplotype
425 (**Figure 3C**). At distances greater than 10kb apart, all demographic models predict there to be
426 more LD than seen in the empirical data (**Figure 3**).

427 We found that the lack of fit is not due to the use of the SMC' approximation in the
428 simulator MaCS (Chen *et al.* 2009), as both MaCS and MSMS (Ewing and Hermisson 2010), a
429 coalescent simulator which does not use the SMC' approximation, yielded highly similar LD
430 decay curves when simulating data under the same simple population contraction model (**Figure**
431 **S3**).

432

433 **SFS predicted by demographic models**

434 Lastly, we examined which of the demographic models could match the SFS of the
435 empirical data. To account for the possibility of overfitting the SFS-based Gutenkunst model to
436 the SFS it was inferred from, we also compared all models to empirical SFSs based on low-
437 coverage high-throughput 1000 Genomes sequence data from the same three populations.

438 *Comparing to the observed Gutenkunst SFS:* For each population, the SFSs predicted by
439 the three MSMC models do not match the empirical proportional SFS from Gutenkunst *et al.*
440 (2009), regardless of the mutation rate or number of genomes used (**Figure 4, S5; Table 1, S2**).
441 The expected SFS based on the Gutenkunst *et al.* (2009) demographic history matches the

442 observed SFS closely, being only 9 log-likelihood units worse than the best possible fit
443 (comparing the empirical SFS to itself) for CEU, 48 units worse for CHB, and 17 units worse for
444 YRI (**Table 1**). In comparison, the best fitting MSMC models for each population are 152, 188
445 and 373 log-likelihood units below the best possible fit (**Table 1**). The combined whole genome
446 plus SFS method SMC++ has an intermediate fit, with a log-likelihood well below the
447 Gutenkunst model, but consistently better than any of the MSMC models (**Table 1**).

448 Interestingly, there is not consistent improvement in fit to the observed SFS when
449 increasing the number of individuals used for the MSMC inference. For each population, the 4-
450 Haplotype model has the worst fit (**Figure 4; Table 1**). For CEU and YRI, the MSMC 2-
451 Haplotype models fit best of the MSMC models, but both are over 100 log-likelihood units
452 worse than the Gutenkunst model. For CHB, the 8-Haplotype model fits best, but is still 140
453 units worse than the Gutenkunst model (**Table 1**).

454 The above comparisons considered the proportions of SNPs at specific frequencies in the
455 sample. We also performed a comparison of the number of SNPs in each bin of the SFS, the
456 absolute SFS, to the observed absolute SFS used in Gutenkunst *et al.*'s (2009) inference using a
457 Poisson likelihood. The absolute SFS expected under the Gutenkunst *et al.* (2009) model fits the
458 observed SFS best (**Figure 5; Table S3**), and is only 9, 49 and 17 log-likelihood units below the
459 best possible fits for CEU, CHB and YRI models, respectively. The SMC++ models have the
460 next best fit to the absolute SFS, but come 86 (CEU), 176 (CHB) and 193 (YRI) log-likelihood
461 units below the best possible fit, followed by MSMC 2-Haplotype which fell 278 (CEU), 378
462 (CHB), and 455 (YRI) below the optimal fit (**Table S3**). In all three populations, the MSMC 4-
463 Haplotype and 8-Haplotype models are thousands of log-likelihood units worse than the best

464 possible fit, showing no improvement based on using a larger number of individuals in the
465 inference (**Table S3**). The over-estimation of SNPs in the 4-Haplotype model is due to the
466 model's extremely high predicted ancestral size (around 200,000 individuals for each population)
467 (**Table S3**).

468 For both the proportional and absolute SFSs, we found that rescaling the models using a
469 higher mutation rate did not produce large qualitative differences in how the MSMC models fit
470 the observed (Gutenkunst) SFS (**Supplementary Note 5; Figure S4-S6**).

471 *Comparing to the folded low-coverage 1000 Genomes SFS:* To avoid giving the Gutenkunst
472 model an unfair advantage by fitting all models to the SFS used to infer that particular model, we
473 also compared all models to proportional folded SFSs based on whole genome and neutral data
474 from the 1000 Genomes project (**Figure 6, S7**). The fit to the empirical singletons bin was poor
475 for all models, except for SMC++, which was, in part, fit to an SFS based on 1000 Genomes
476 data. Calling singletons is notoriously difficult in low-coverage data, making that bin the least
477 reliable in the 1000 Genomes data (Kim *et al.* 2011; Nielsen *et al.* 2011; Han *et al.* 2014; 2015).
478 We therefore calculated likelihoods for all models relative to the data both with singletons
479 included and again with the SFSs renormalized without the singletons category (**Figure S7;**
480 **Table S4**).

481 For YRI, the Gutenkunst model is the best fitting model for the whole genome and
482 neutral 1000 Genomes SFSs, both with and without singletons, with all other models having a
483 much worse fit (the next best model, SMC++, is hundreds to thousands of log-likelihood units
484 below the fit of the Gutenkunst model) (**Figure 6C; Table S4**). For CEU and CHB, if singletons
485 are included, SMC++ fits the whole genome and neutral 1000 Genomes SFSs best. For CEU, the

486 Gutenkunst model then fits second-best, with the MSMC models far behind (**Figure 6A; Table**
487 **S4**). For CHB, the MSMC 2-Haplotype fits second-best after SMC++, with the Gutenkunst
488 model coming third, but both are over 10,000 log-likelihood units below SMC++ (**Figure 6B;**
489 **Table S4**). If singletons are excluded for CEU and CHB, then the Gutenkunst model fits best,
490 with SMC++ coming in second, and the MSMC models all ranking far below (**Table S4**).

491

492 **Effect of Uncertain Ancestral Population Size**

493 The accuracy of ancient ancestral population sizes, particularly more than 3 million years
494 (>100,000 generations) ago, using the whole genome-based methods remains unclear (Li and
495 Durbin 2011). As discussed above, the MSMC 2-Haplotype and 4-Haplotype models infer large
496 ancestral sizes for each population that are not supported by previous inferences of human
497 demographic history (Adams and Hudson 2004; Keinan *et al.* 2007; Boyko *et al.* 2008;
498 Gutenkunst *et al.* 2009; Nielsen *et al.* 2009; Gravel *et al.* 2011). We hypothesized that these
499 extreme ancestral sizes, as well as ancient bottlenecks and population growth (the signature
500 “humps” of MSMC trajectories), which do not appear in demographic models inferred using
501 other methods, could be artifacts that are causing the SFS predicted by these models to deviate
502 from the true SFS.

503 To test this hypothesis, we took the best fitting of the MSMC models, the CEU 2-
504 Haplotype model, and carried out a series of adjustment experiments to determine whether
505 changes to the model could provide a better fit to the observed SFS. Without adjusting the time
506 period encompassed by the model, we altered the ancestral population size to a variety of values
507 including those inferred by Gutenkunst *et al.* (2009) (**Supplementary Note 7; Figure S10-S11**).

508 We also truncated the MSMC trajectory to remove ancient events and better match the time
509 period (in years) encompassed by the Gutenkunst *et al.* (2009) model. We again adjusted the
510 ancestral population size to a variety of plausible values (**Supplementary Note 7; Figure S12-**
511 **S13**).

512 We found trimming away the ancient (older than ~225k years ago) part of the
513 demographic trajectory and lowering the ancestral population size to 10,000 – 12,300 (compared
514 to 41,261 inferred initially) dramatically improved the fit of the proportional SFSs predicted
515 under these adjusted models to the Observed (Gutenkunst) SFS (**Figure S12; Table S5**). The
516 best-fit model with ancestral size (N_A) equal to 12,300 was brought to within 38 log likelihood
517 units of the best possible likelihood (**Figure S12D; Table S5**), only 29 units below the
518 Gutenkunst model. When repeating this procedure using the SFS based on counts, the SFSs
519 under these adjusted models showed a different pattern of improvement. Here the untrimmed
520 models that did *not* have ancient events >225 kya trimmed away, but had a lowered ancestral
521 population size of 7,300-12,300, showed the most improvement (**Figure S11-S12**). However,
522 their fit was still more than 100 log-likelihood units worse than the Gutenkunst model (**Figure**
523 **S12; Table S6**).

524

525 **MSMC Population Size Trajectories for Demographic Models Inferred from the SFS**

526 Given that the SFSs predicted by the demographic models inferred using MSMC do not
527 fit the observed SFS, we examined whether MSMC is capable of recovering a complex
528 demography such as the one inferred by Gutenkunst *et al.* (2009) from a single simulated
529 genome. We find that MSMC performs relatively well at inferring the underlying demography

530 from the simulated data. **Figure 7A** shows the underlying Gutenkunst demographic model for
531 each population (purple) (as in the other Gutenkunst model simulations, migration is included in
532 the model, but is not depicted in our diagrams), with the results of 50 independent MSMC
533 inferences on each 2-Haplotype simulated dataset coming close to the underlying demography.
534 However, sharp bottlenecks are inferred as long population declines (as noted by Li and Durbin
535 (2011) and Schiffels and Durbin (2014)). Additionally, we found evidence of MSMC detecting a
536 false spurt of growth in the YRI population 1350 generations ago (**Figure 7A**). Both of these
537 phenomena were also noted by Bunnfeld *et al.* (2015).

538 The SFSs predicted by the demographic models inferred using MSMC on the simulated
539 data fit the SFS expected under the Gutenkunst model and the observed Gutenkunst SFSs better
540 than the MSMC demographic models inferred by Schiffels and Durbin (2014) (**Figure 7B-C**).
541 The proportional MSMC simulated data SFSs were only 40, 74 and 10 log-likelihood units
542 below the Gutenkunst model SFS (**Table S2**), with the SFSs based on SNP counts showing a
543 similar pattern (**Table S3**). Therefore, if the Gutenkunst model is the true demographic model for
544 human history, MSMC accurately captures the population size changes and produces an
545 appropriate SFS.

546 It is well established that 2-haplotype whole genome-based inference (PSMC, MSMC 2-
547 Haplotype, also known as PSMC') is not able to detect recent demographic events (Li and
548 Durbin 2011; Schiffels and Durbin 2014). However, the ability to detect recent growth by using
549 more than two haplotypes in the inference is cited as a feature of MSMC (Schiffels and Durbin
550 2014). We ran MSMC 2-Haplotype and 8-Haplotype on datasets simulated under the Gutenkunst
551 model and a Gutenkunst model plus extreme recent growth (**Supplementary Note 6; Figure**

552 **S8**). Unsurprisingly, MSMC 2-Haplotype was not able to detect extreme recent growth. Its
553 estimates of current population size were fairly accurate for the original Gutenkunst model
554 (**Figure 7A**), but the method dramatically underestimated the growth for data simulated under
555 the Gutenkunst + Growth model (**Figure S8**). The results from 8-Haplotype MSMC inference
556 were most surprising. We found that for both models, MSMC 8-Haplotype inferred extreme
557 recent growth as many as four orders of magnitude beyond that in the underlying model, with a
558 high degree of variance between replicates (**Figure S8**). Despite the high degree of variance, the
559 average of the MSMC trajectories all showed a strong upward bias in estimates of the recent past
560 (**Figure S8**). While the ability to detect recent growth is meant to be a feature of MSMC, our
561 findings indicate that the magnitude of growth may not be estimated well.

562 We had hypothesized that Neanderthal admixture could cause deviation between the
563 MSMC and Gutenkunst demographic models, but found that the addition of Neanderthal
564 admixture to our Gutenkunst model simulations did not substantively change the MSMC
565 trajectories or expected SFSs (**Supplementary Note 6; Figure S9; Table S2, S3**).

566

567

DISCUSSION

568 We tested which published models of human demographic history, inferred using either
569 whole genome sequence data, the SFS, or a combined approach, can recapitulate multiple
570 summaries of human genetic variation data. We found that no model was able to recapitulate all
571 summaries of the data, but some models still performed better than others. In particular, none of
572 the models was able to recapitulate LD decay, but the Gutenkunst SFS-based models and the
573 combined whole genome and SFS-based SMC++ models were able to recapitulate empirical

574 heterozygosity and the SFS. MSMC 2-Haplotype was able to recapitulate heterozygosity, but not
575 the SFS, and MSMC 4-Haplotype and 8-Haplotype could fit neither heterozygosity nor the SFS,
576 though MSMC 8-Haplotype did fit LD decay slightly better than the other models. These results
577 highlight the uncertainties of demographic inference from one, or even two, types of data and the
578 need to assess the fit of demographic models using multiple summaries of the data.

579 We found that the models based on MSMC inference from 4 or 8 haplotypes did not
580 improve the fit of the expected SFS compared to that based on two haplotypes; in fact, in most
581 cases the 4- and 8-Haplotype models fit much worse than the 2-Haplotype models. The 4-
582 Haplotype models for CEU, CHB and YRI and the 8-Haplotype model for YRI appear to fit
583 poorly due to their extremely high ancestral sizes and ancient humps of growth and decline
584 (**Figure 1**). The expected SFSs under the 8-Haplotype models for CEU and CHB show a skew
585 toward low-frequency variants that may be due to their low ancestral size followed by extreme
586 recent growth (**Figure 1**). We find that MSMC 8-Haplotype vastly overestimates recent growth
587 in simulated data, which may be contributing to the lack of fit to the SFS (**Figure S8**). This result
588 is at odds with the findings of Schiffels and Durbin (2014), who suggested that using eight
589 haplotypes instead of two should increase accuracy of population size inference in the recent
590 past, though they also noted a bias toward smaller ancient population sizes when using an
591 increased number of haplotypes. Changing the scaling of the mutation rate did not generally help
592 the MSMC models to fit the expected SFS better (**Figure S4-S6**). It is worth noting that the
593 model inferred in SMC++ used the same mutation rate as MSMC, yet fit the empirical SFSs
594 much better (**Figure 4-6; Table 1, S2-S4**), indicating that mutation rate differences between the
595 whole genome and SFS-based studies is not the source of the discrepancies.

596 We found that in addition to not fitting the empirical SFS, the MSMC 4-Haplotype and 8-
597 Haplotype models did not predict the genome-wide distribution of heterozygosity (**Figure 2**)
598 which may be surprising as the genome-wide distribution of heterozygosity is a major feature of
599 the data used by MSMC. The reason for the lack of fit for these models appears to be the
600 extremely high ancestral size inferred in the 4-Haplotype models for all three populations and in
601 the 8-Haplotype YRI model, and the low ancestral size inferred in the 8-Haplotype Models for
602 CEU and CHB (**Figure 1**).

603 Since the most ancient size in the MSMC trajectory will have a large influence on
604 heterozygosity and the SFS and the most ancient bin of the MSMC trajectory may be unreliable
605 (Li and Durbin 2011; Schiffels and Durbin 2014), we explored the effect of altering this ancient
606 size and removing ancient growth events in the CEU MSMC 2-Haplotype model. We found that
607 selective trimming could improve the fit to the SFS (**Figure S10-S13**). However, the final bin of
608 the model cannot explain all of the lack of fit of the MSMC models to the data as the CEU and
609 CHB MSMC 8-Haplotype trajectories do not show the extreme ancestral sizes in the last bin, yet
610 these models also dramatically deviate from empirical heterozygosity and the SFS. In other
611 words, simple exclusion of the final high ancestral size is not sufficient to improve model fit to
612 other summaries of the data. Our trimming experiments were only made possible by the
613 abundance of human sequence data and demographic models previously fit to the data. Since
614 many MSMC trajectories are calculated for species for which there is no prior information about
615 ancient demographic history, the “informed trimming” we carried out is not a practicable
616 solution to improve the reliability of MSMC inference.

617 While our results indicate that features of MSMC trajectories, particularly ancient events,
618 should be regarded with caution, we also found that MSMC 2-Haplotype is able to accurately
619 recapitulate a complex demography (with the exception of steep drops in population size,
620 extreme recent growth, and some false periods of growth) from simulated data, supporting the
621 validity of the method, at least for use on simulated data (**Figure 7**). Migration between
622 populations did not appear to cause deviations in MSMC trajectories from the underlying model
623 (**Figure 7**), nor did a small degree of Neanderthal admixture (**Figure S9**), indicating that MSMC
624 is robust to small amounts of gene flow. The fact that the 2-Haplotype model based on real data
625 did not fit the observed SFS very well (**Figure 4-6; Table 1, S2-S4**) suggests that the true
626 underlying pattern of human demography is more complex than either type of inference ($\partial\text{a}\partial\text{i}$ or
627 MSMC) is capturing, potentially revealing weaknesses in both methods.

628 Alternatively, if the Gutenkunst *et al.* (2009) demographic model is largely accurate,
629 biases or other factors that exist in real data but not in simulated data may be affecting MSMC
630 inference, resulting in the method failing to recover an underlying demography that matches
631 Gutenkunst *et al.*'s (2009) model. For example, Song *et al.* (2016) found that statistical phasing
632 could affect MSMC estimates of population split times, and Nadachowska-Brzyska *et al.* (2016)
633 found that per-site sequencing depth, mean genome coverage and the amount of missing data led
634 to differences in PSMC curve amplitudes, expansions and contractions, and the timing and
635 values of N_e . They therefore recommended only using samples with a mean genome coverage of
636 $\geq 18X$ and $< 25\%$ missing data, and employing a per-site sequencing depth filter of ≥ 10
637 (Nadachowska-Brzyska *et al.* 2016). The Complete Genomics genomes used by Li & Durbin
638 (2011) were $> 40X$ coverage (Drmanac *et al.* 2010), indicating that lack of coverage is not

639 responsible for their divergence from estimates based on the SFS. However, the standards
640 suggested by Nadachowska-Brzyska (2016) may not always be attainable in *de novo* genome
641 projects, and thus, data quality issues may affect non-model organism PSMC and MSMC
642 inferences more acutely. Future work should also examine the impact of artifacts of genome
643 assembly errors and structural variants on PSMC inference. For example, collapsing duplicate
644 regions of the genome on top of each other could result in regions of the genome having excess
645 heterozygosity, which could in turn affect inference of demography.

646 We found that no model was able to accurately recapitulate the empirical distribution of
647 LD decay. The lack of fit of the SFS-based models is perhaps unsurprising, as Harris & Nielsen
648 (Harris and Nielsen 2013) found that the Gutenkunst model cannot recapitulate empirical IBS
649 distributions (a finer-scale summary of the data related to LD), and Garud et al. (Garud *et al.*
650 2015) found that they could not recover empirical LD patterns in *Drosophila*, despite matching
651 the SFS, number of segregating sites (S) and number of pairwise differences (π). Garud et al.
652 (Garud *et al.* 2015) suggested the lack of fit could either be due to linked positive selection or to
653 an incompleteness of the demographic model, demonstrating how models that fit some
654 summaries of the data may not recapitulate others. It is more surprising that the MSMC 2-
655 Haplotype and 4-Haplotype models do not fit the data well, as the method uses LD information
656 in its inference, though different summaries of LD may be affected by demography in distinct
657 ways (Plagnol and Wall 2006). Other possible factors that could lead to the lack of fit of all
658 models to empirical LD decay patterns include the absence of natural selection, gene conversion,
659 and fine-scale recombination hotspots in our simulations (Ardlie *et al.* 2001; Frisse *et al.* 2001;
660 Wall and Pritchard 2003). Further, if the true mutation rate is actually smaller than the relatively

661 high value used by Gutenkunst et al. ($\mu = 2.35 \times 10^{-8}$ mutations/bp/generation), then the
662 population sizes would have to be larger than those estimated by Gutenkunst et al. (2009). Larger
663 population sizes would yield larger values of the population scaled recombination rate (ρ) than
664 what was used in our simulations under the Gutenkunst model. Larger values of ρ would then
665 lead to a decrease in LD in the simulations, which might better match the empirical LD decay
666 curves.

667 Natural selection may affect both SFS and whole genome based methods of demographic
668 inference. Li and Durbin (Li and Durbin 2011) found that masking exonic sequence did not alter
669 PSMC trajectories. However, Schrider *et al.* (2016) examined the impact of selective sweeps on
670 demographic inference using the SFS in $\partial a \partial i$, approximate Bayesian computation (ABC), and
671 PSMC and found that all three methods were influenced to varying degrees and in slightly
672 different directions by the presence of selective sweeps, with $\partial a \partial i$ the most robust to these
673 effects. This is a concern for published human demographic models as Gutenkunst *et al.* (2009)
674 used noncoding sequence from autosomal genes in their study, which may be subject to linked
675 selection (Gazave *et al.* 2014; Schrider *et al.* 2016). Schiffels and Durbin (2014) used whole
676 genome sequences that included genic and non-genic regions some of which are certainly under
677 selection. Thus, the sensitivity of these methods to selection may partially explain why both
678 perform well on simulated data without selection, yet have such divergent results when run on
679 empirical data.

680 Our results have implications for understanding human demographic history. First, there
681 has been controversy concerning the presence of ancient bottlenecks (>100 kya) in human
682 populations (Takahata *et al.* 1995; Harpending *et al.* 1998; Takahata and Satta 1998; Hawks *et*

683 *al.* 2000; Garrigan and Hammer 2006; Fagundes *et al.* 2007; Scholz *et al.* 2007; Blum and
684 Jakobsson 2011; Sjödin *et al.* 2012). The inferred “humps” in the ancient portions of MSMC
685 plots (**Figure 1**) tended to lend support to these ancient population size changes that appeared to
686 be absent from SFS demographic estimates. Our results suggest that if these ancient population
687 size changes did indeed occur, the resulting SFS would appear very different from the SFSs seen
688 in human populations (**Figure 4-6, S10-S13**). The fact that they are not seen in the observed SFS
689 suggests that either the size changes did not occur, and the inferred size changes are artifacts, or
690 instead, the true demography is more complex than currently modeled using either approach. Our
691 conclusion of finding little evidence for the ancient population size changes is supported by the
692 study of Sjödin *et al.* (2012). They employed an approximate Bayesian computation approach to
693 directly test models with ancient population size changes in Africa and found little support for
694 such ancient bottlenecks.

695 Deep ancestral structure has been put forward as explanation for the humps detected by
696 the whole genome-based methods by the developers of PSMC and others (Li and Durbin 2011;
697 Henn *et al.* 2012; Mazet, Rodriguez, and Chikhi 2015; Mazet, Rodriguez, Grusea, *et al.* 2015;
698 Orozco-terWengel 2016). While Blum and Jakobssen (2011) used the TMRCA to postulate an
699 ancient bottleneck 150-kya, they also were not able to a reject a model of ancestral structure.
700 Strikingly, Mazet *et al.* (2015) were able to perfectly recapitulate the human PSMC humps
701 without invoking a single size change in the population by simulating data from a highly
702 structured ancestral population (10 sub-populations) and modulating the amount of gene flow
703 between these populations. Therefore, the large ‘population size changes’ inferred in MSMC,
704 which cause the models not to match the empirical SFS, may in fact be due to complex structure

705 and large-scale changes in gene flow. This ancient structure may have a large effect on MSMC
706 trajectories and LD patterns, but may not strongly influence the SFS (see Figure 7 in Lohmueller
707 *et al.* (2009)), potentially resolving the discrepancy between the methods (Henn *et al.* 2012).

708 Our work provides a cautionary tale for understanding population history in non-model
709 organisms. Our results argue against a literal interpretation of “humps” and other jumps in
710 MSMC plots as reflecting population size changes. This problem is exacerbated for putative
711 ancient size changes. Given the ever-increasing generation of genomic data from non-model taxa
712 and the application of whole genome-based approaches to such data (Meyer *et al.* 2012; Groenen
713 *et al.* 2012; Zhao *et al.* 2012; Albert *et al.* 2013; Ibarra-Laclette *et al.* 2013; Orlando *et al.* 2013;
714 Prado-Martinez *et al.* 2013; Nadachowska-Brzyska *et al.* 2013; Bosse *et al.* 2014; Freedman *et*
715 *al.* 2014; Prufer *et al.* 2014; Hung *et al.* 2014; Nadachowska-Brzyska *et al.* 2015; Palkopoulou *et*
716 *al.* 2015; Holliday *et al.* 2016; Nadachowska-Brzyska *et al.* 2016; Wang *et al.* 2016), our
717 findings are especially concerning. We recommend employing other model-based types of
718 demographic inference leveraging either SFS-based or other summary statistics in an ABC
719 framework to test whether important demographic features suggested by PSMC or MSMC plots
720 can be recapitulated using other features in the data. We also recommend, as done in Thornton
721 and Andolfatto (2006), Freedman *et al.* (2014), Song *et al.* (2016), Hsieh (2016) and Cahill *et al.*
722 (2016) that the PSMC or MSMC plots and TMRCA estimates be used themselves as summary
723 statistics for model comparison, rather than the actual population size estimates. In other words,
724 more complex demographic models can be simulated and tested to see whether they recapitulate
725 the observed whole genome-based trajectories. Of course, this approach will not be successful if
726 the trajectories are strongly influenced by bioinformatics artifacts or other features not captured

727 within the simulations, such as natural selection. For both PSMC/MSMC and SFS-based
728 inference methods, we also recommend testing whether the estimated models can predict
729 multiple features of the data. Specifically, researchers should check whether their inferred model
730 can recapitulate the genome-wide distribution of heterozygosity. The genome-wide distribution
731 of heterozygosity may be the most practical and useful statistic for studies of non-model
732 organisms that only have a handful of genomes available to them. SMC++ and other new
733 approaches that leverage multiple types of data (Bunnefeld *et al.* 2015; Boitard *et al.* 2016;
734 Weissman and Hallatschek 2017) are promising alternatives, though our results indicate that
735 SMC++ still cannot recapitulate all summaries of the data.

736 Testing more complex demographic scenarios using multiple summaries of the data may
737 help to resolve uncertainties about our own species' history and will improve demographic
738 inference for non-model organisms. Incorporating the potential complexity of possible
739 demographic histories to produce models that better recapitulate the data may in fact present the
740 greatest challenge.

741

742

ACKNOWLEDGEMENTS

743

We thank Ryan Gutenkunst for providing us with the SFS from his paper, and Yun Song

744

for his published demographic models. We also thank Diego Ortega Del Vecchyo and Bernard

745

Kim for advice, and Christian Huber, Robert K. Wayne and Emilia Huerta-Sanchez for helpful

746

comments on the manuscript. Joshua Schraiber and several anonymous reviewers made many

747

insightful comments that strengthened our manuscript. This work was supported by National

748

Institutes of Health (NIH) grant R35GM119856 to KEL and NIH Training Grant in Genomic

749

Analysis and Interpretation T32HG002536 and National Science Foundation Graduate Research

750

Fellowship Program to ACB. TNP was supported by National Institute of Health, under Ruth L.

751

Kirschstein National Research Service Award (T32-GM008185).

752

753

754

TABLES

755

756 **Table 1: Multinomial log-likelihoods comparing the fit of various models to the observed**757 **SFS derived from Sanger sequencing data and used by Gutenkunst *et al.* (2009) for their**758 **inference (SFSs in Figure 4)**

759

CEU		
Model	Multinomial LL	Δ LL (Model - Data)
Data to Data ^a	-21546	0
Gutenkunst ^b	-21555	-9
SMC++ ^c	-21599	-53
MSMC 2-Hap ^d	-21698	-152
MSMC 8-Hap ^d	-21816	-270
MSMC 4-Hap ^d	-22760	-1214
CHB		
Model	Multinomial LL	Δ LL (Model - Data)
Data to Data	-20154	0
Gutenkunst	-20202	-48
SMC++	-20277	-123
MSMC 8-Hap	-20343	-188
MSMC 2-Hap	-20370	-216
MSMC 4-Hap	-21411	-1257
YRI		
Model	Multinomial LL	Δ LL (Model - Data)
Data to Data	-29630	0
Gutenkunst	-29647	-17
SMC++	-29779	-150
MSMC 2-Hap	-30003	-373
MSMC 8-Hap	-31282	-1652
MSMC 4-Hap	-32976	-3346

760

761 ^aDenotes the best log-likelihood possible when replacing the proportions predicted by the model with the
762 observed proportions from the SFS used in Gutenkunst *et al.*'s (2009) study (see **Supplementary Note**
763 **4**).

764 ^bDenotes the model inferred by Gutenkunst *et al.* (2009) fit to the observed SFS

765 ^cDenotes the model inferred by Terhorst *et al.* (2017) using a combined whole genome and SFS
766 approach

767 ^dDenotes the demographic models inferred by Schiffels and Durbin (2014) using MSMC on 2, 4 and 8
768 haplotypes

769

770

REFERENCES

771 1000 Genomes Project Consortium, 2015 A global reference for human genetic variation. *Nature*
772 526: 68–74.

773 Adams, A. M., and R. R. Hudson, 2004 Maximum-likelihood estimation of demographic
774 parameters using the frequency spectrum of unlinked single-nucleotide polymorphisms.
775 *Genetics* 168: 1699–1712.

776 Albert, V. A., W. B. Barbazuk, J. P. Der, J. Leebens-Mack, H. Ma *et al.*, 2013 The *Amborella*
777 genome and the evolution of flowering plants. *Science* 342: 1241089.

778 Arbiza, L., E. Zhong, and A. Keinan, 2012 NRE: a tool for exploring neutral loci in the human
779 genome. *BMC Bioinformatics* 13: 301.

780 Ardlie, K., S. N. Liu-Cordero, M. A. Eberle, M. Daly, J. Barrett *et al.*, 2001 Lower-than-
781 expected linkage disequilibrium between tightly linked markers in humans suggests a role
782 for gene conversion. *Am J Hum Genet* 69: 582–589.

783 Bhaskar, A., Y. R. Wang, and Y. S. Song, 2015 Efficient inference of population size histories
784 and locus-specific mutation rates from large-sample genomic variation data. *Genome Res*
785 25: 268–279.

786 Blum, M. G., and M. Jakobsson, 2011 Deep divergences of human gene trees and models of
787 human origins. *Mol Biol Evol* 28: 889–898.

788 Boitard, S., W. Rodriguez, F. Jay, S. Mona, and F. Austerlitz, 2016 Inferring population size
789 history from large samples of genome-wide molecular data-an approximate Bayesian
790 computation approach. *PLoS Genet* 12: e1005877.

791 Bosse, M., H.-J. Megens, O. Madsen, L. A. Frantz, Y. Paudel *et al.*, 2014 Untangling the hybrid
792 nature of modern pig genomes: a mosaic derived from biogeographically distinct and highly
793 divergent *Sus scrofa* populations. *Mol Ecol* 23: 4089–4102.

794 Boyko, A. R., S. H. Williamson, A. R. Indap, J. D. Degenhardt, R. D. Hernandez *et al.*, 2008
795 Assessing the evolutionary impact of amino acid mutations in the human genome. *PLoS*
796 *Genet* 4: e1000083.

797 Bunnefeld, L., L. A. F. Frantz, and K. Lohse, 2015 Inferring bottlenecks from genome-wide
798 samples of short sequence blocks. *Genetics* 201: 1157–1169.

799 Cahill, J. A., A. E. Soares, R. E. Green, and B. Shapiro, 2016 Inferring species divergence times
800 using pairwise sequential Markovian coalescent modelling and low-coverage genomic data.
801 *Philos Trans R Soc London [Biol]* 371: 20150138.

802 Chen, G. K., P. Marjoram, and J. D. Wall, 2009 Fast and flexible simulation of DNA sequence

803 data. *Genome Res* 19: 136–142.

804 Chikhi, L., V. C. Sousa, P. Luisi, B. Goossens, and M. A. Beaumont, 2010 The confounding
805 effects of population structure, genetic diversity and the sampling scheme on the detection
806 and quantification of population size changes. *Genetics* 186: 983–995.

807 Danecek, P., A. Auton, G. Abecasis, C. A. Albers, E. Banks *et al.*, 2011 The variant call format
808 and VCFtools. *Bioinformatics* 27: 2156–2158.

809 Drmanac, R., A. B. Sparks, M. J. Callow, A. L. Halpern, N. L. Burns *et al.*, 2010 Human genome
810 sequencing using unchained base reads on self-assembling DNA nanoarrays. *Science* 327:
811 78–81.

812 Ewing, G., and J. Hermisson, 2010 MSMS: a coalescent simulation program including
813 recombination, demographic structure and selection at a single locus. *Bioinformatics* 26:
814 2064–2065.

815 Excoffier, L., I. Dupanloup, E. Huerta-Sánchez, V. C. Sousa, and M. Foll, 2013 Robust
816 demographic inference from genomic and SNP data. *PLoS Genet* 9: e1003905.

817 Fagundes, N. J., N. Ray, M. Beaumont, S. Neuenschwander, F. M. Salzano *et al.*, 2007
818 Statistical evaluation of alternative models of human evolution. *Proc Natl Acad Sci USA*
819 104: 17614–17619.

820 Fitak, R. R., E. Mohandesan, J. Corander, and P. A. Burger, 2016 The de novo genome assembly
821 and annotation of a female domestic dromedary of North African origin. *Molecular Ecology*
822 *Resources* 16: 314–324.

823 Freedman, A. H., I. Gronau, R. M. Schweizer, D. Ortega-Del Vecchyo, E. Han *et al.*, 2014
824 Genome sequencing highlights the dynamic early history of dogs. *PLoS Genet* 10:
825 e1004016.

826 Frisse, L., R. R. Hudson, A. Bartoszewicz, J. D. Wall, J. Donfack *et al.*, 2001 Gene conversion
827 and different population histories may explain the contrast between polymorphism and
828 linkage disequilibrium levels. *Am J Hum Genet* 69: 831–843.

829 Gao, F., and A. Keinan, 2016 Explosive genetic evidence for explosive human population
830 growth. *Curr Opin Genetics Dev* 41: 130–139.

831 Garrigan, D., and M. F. Hammer, 2006 Reconstructing human origins in the genomic era. *Nature*
832 *Rev Genet* 7: 669–680.

833 Garud, N. R., P. W. Messer, E. O. Buzbas, and D. A. Petrov, 2015 Recent selective sweeps in
834 North American *Drosophila melanogaster* show signatures of soft sweeps. *PLoS Genet* 11:
835 e1005004.

- 836 Gattepaille, L. M., M. Jakobsson, and M. G. Blum, 2013 Inferring population size changes with
837 sequence and SNP data: lessons from human bottlenecks. *Heredity* 110: 409–419.
- 838 Gazave, E., D. Chang, A. G. Clark, and A. Keinan, 2013 Population growth inflates the per-
839 individual number of deleterious mutations and reduces their mean effect. *Genetics* 195:
840 969–978.
- 841 Gazave, E., L. Ma, D. Chang, A. Coventry, F. Gao *et al.*, 2014 Neutral genomic regions refine
842 models of recent rapid human population growth. *Proc Natl Acad Sci USA* 111: 757–762.
- 843 Gravel, S., B. M. Henn, R. N. Gutenkunst, A. R. Indap, G. T. Marth *et al.*, 2011 Demographic
844 history and rare allele sharing among human populations. *Proc Natl Acad Sci USA* 108:
845 11983–11988.
- 846 Groenen, M. A. M., A. L. Archibald, H. Uenishi, C. K. Tuggle, Y. Takeuchi *et al.*, 2012
847 Analyses of pig genomes provide insight into porcine demography and evolution. *Nature*
848 491: 393–398.
- 849 Gutenkunst, R. N., R. D. Hernandez, S. H. Williamson, and C. D. Bustamante, 2009 Inferring the
850 joint demographic history of multiple populations from multidimensional SNP frequency
851 data. *PLoS Genet* 5: e1000695.
- 852 Han, E., J. S. Sinsheimer, and J. Novembre, 2014 Characterizing bias in population genetic
853 inferences from low-coverage sequencing data. *Mol Biol Evol* 31: 723–735.
- 854 Han, E., J. S. Sinsheimer, and J. Novembre, 2015 Fast and accurate site frequency spectrum
855 estimation from low coverage sequence data. *Bioinformatics* 31: 720–725.
- 856 Harpending, H. C., M. A. Batzer, M. Gurven, L. B. Jorde, A. R. Rogers *et al.*, 1998 Genetic
857 traces of ancient demography. *Proc Natl Acad Sci USA* 95: 1961–1967.
- 858 Harris, K., and R. Nielsen, 2013 Inferring demographic history from a spectrum of shared
859 haplotype lengths. *PLoS Genet* 9: e1003521.
- 860 Hawks, J., K. Hunley, S.-H. Lee, and M. Wolpoff, 2000 Population bottlenecks and Pleistocene
861 human evolution. *Mol Biol Evol* 17: 2–22.
- 862 Heller, R., L. Chikhi, and H. R. Siegismund, 2013 The confounding effect of population
863 structure on Bayesian skyline plot inferences of demographic history. *PLoS ONE* 8: 1–10.
- 864 Henn, B. M., L. R. Botigué, S. Peischl, I. Dupanloup, M. Lipatov *et al.*, 2016 Distance from sub-
865 Saharan Africa predicts mutational load in diverse human genomes. *Proc Natl Acad Sci USA*
866 113: E440–E449.
- 867 Henn, B. M., L. L. Cavalli-Sforza, and M. W. Feldman, 2012 The great human expansion. *Proc*
868 *Natl Acad Sci USA* 109: 17758–17764.

- 869 Holliday, J. A., L. Zhou, R. Bawa, M. Zhang, and R. W. Oubida, 2016 Evidence for extensive
870 parallelism but divergent genomic architecture of adaptation along altitudinal and latitudinal
871 gradients in *Populus trichocarpa*. *New Phytologist* 209: 1240–1251.
- 872 Hsieh, P., K. R. Veeramah, J. Lachance, S. A. Tishkoff, J. D. Wall *et al.*, 2016 Whole-genome
873 sequence analyses of Western Central African Pygmy hunter-gatherers reveal a complex
874 demographic history and identify candidate genes under positive natural selection. *Genome*
875 *Res* 26: 279–290.
- 876 Hudson, R. R., 2002 Generating samples under a Wright–Fisher neutral model of genetic
877 variation. *Bioinformatics* 18: 337–338.
- 878 Hung, C.-M., P.-J. L. Shaner, R. M. Zink, W.-C. Liu, T.-C. Chu *et al.*, 2014 Drastic population
879 fluctuations explain the rapid extinction of the passenger pigeon. *Proc Natl Acad Sci USA*
880 111: 10636–10641.
- 881 Ibarra-Laclette, E., E. Lyons, G. Hernández-Guzmán, C. A. Pérez-Torres, L. Carretero-Paulet *et*
882 *al.*, 2013 Architecture and evolution of a minute plant genome. *Nature* 498: 94–98.
- 883 Jouganous, J., W. Long, A. P. Ragsdale, and S. Gravel, 2017 Inferring the Joint Demographic
884 History of Multiple Populations: Beyond the Diffusion Approximation. *Genetics genetics*.
885 117.200493.
- 886 Keinan, A., and A. G. Clark, 2012 Recent explosive human population growth has resulted in an
887 excess of rare genetic variants. *Science* 336: 740–743.
- 888 Keinan, A., J. C. Mullikin, N. Patterson, and D. Reich, 2007 Measurement of the human allele
889 frequency spectrum demonstrates greater genetic drift in East Asians than in Europeans. *Nat*
890 *Genet* 39: 1251–1255.
- 891 Kidd, J. M., S. Gravel, J. Byrnes, A. Moreno-Estrada, S. Musharoff *et al.*, 2012 Population
892 genetic inference from personal genome data: impact of ancestry and admixture on human
893 genomic variation. *Am J Hum Genet* 91: 660–671.
- 894 Kim, S. Y., K. E. Lohmueller, A. Albrechtsen, Y. Li, T. Korneliussen *et al.*, 2011 Estimation of
895 allele frequency and association mapping using next-generation sequencing data. *BMC*
896 *Bioinformatics* 12: 231.
- 897 Kong, A., G. Thorleifsson, D. F. Gudbjartsson, G. Masson, A. Sigurdsson *et al.*, 2010 Fine-scale
898 recombination rate differences between sexes, populations and individuals. *Nature* 467:
899 1099–1103.
- 900 Li, H., and R. Durbin, 2011 Inference of human population history from individual whole-
901 genome sequences. *Nature* 475: 493–496.
- 902 Liu, X., and Y.-X. Fu, 2015 Exploring population size changes using SNP frequency spectra. *Nat*

- 903 Genet 47: 555–559.
- 904 Lohmueller, K. E., C. D. Bustamante, and A. G. Clark, 2009 Methods for human demographic
905 inference using haplotype patterns from genomewide single-nucleotide polymorphism data.
906 Genetics 182: 217–231.
- 907 Malaspinas, A. S., M. C. Westaway, C. Muller, V. C. Sousa, O. Lao *et al.*, 2016 A genomic
908 history of Aboriginal Australia. Nature 538: 207–214.
- 909 Mallick, S., H. Li, M. Lipson, I. Mathieson, M. Gymrek *et al.*, 2016 The Simons Genome
910 Diversity Project: 300 genomes from 142 diverse populations. Nature 538: 201–206.
- 911 Marjoram, P., and J. D. Wall, 2006 Fast “coalescent” simulation. BMC Genet 7: 1–9.
- 912 Marth, G. T., E. Czabarka, J. Murvai, and S. T. Sherry, 2004 The allele frequency spectrum in
913 genome-wide human variation data reveals signals of differential demographic history in
914 three large world populations. Genetics 166: 351–372.
- 915 Mazet, O., W. Rodriguez, and L. Chikhi, 2015 Demographic inference using genetic data from a
916 single individual: Separating population size variation from population structure. Theor
917 Popul Biol 104: 46–58.
- 918 Mazet, O., W. Rodriguez, S. Grusea, S. Boitard, and L. Chikhi, 2015 On the importance of being
919 structured: instantaneous coalescence rates and human evolution—lessons for ancestral
920 population size inference? Heredity 116: 362–371.
- 921 McCoy, R. C., N. R. Garud, J. L. Kelley, C. L. Boggs, and D. A. Petrov, 2014 Genomic
922 inference accurately predicts the timing and severity of a recent bottleneck in a nonmodel
923 insect population. Mol Ecol 23: 136–150.
- 924 McVean, G. A., and N. J. Cardin, 2005 Approximating the coalescent with recombination. Philos
925 Trans R Soc London [Biol] 360: 1387–1393.
- 926 Meyer, M., M. Kircher, M.-T. Gansauge, H. Li, F. Racimo *et al.*, 2012 A high-coverage genome
927 sequence from an archaic Denisovan individual. Science 338: 222–226.
- 928 Murray, G. G. R., A. E. R. Soares, B. J. Novak, N. K. Schaefer, J. A. Cahill *et al.*, 2017 Natural
929 selection shaped the rise and fall of passenger pigeon genomic diversity. bioRxiv
930 <http://biorxiv.org/lookup/doi/10.1101/154294>.
- 931 Nadachowska-Brzyska, K., R. Burri, P. I. Olason, T. Kawakami, L. A. Smeds *et al.*, 2013
932 Demographic divergence history of pied flycatcher and collared flycatcher inferred from
933 whole-genome re-sequencing data. PLoS Genet 9: e1003942.
- 934 Nadachowska-Brzyska, K., R. Burri, L. Smeds, and H. Ellegren, 2016 PSMC analysis of
935 effective population sizes in molecular ecology and its application to black-and-white

- 936 *Ficedula* flycatchers. *Mol Ecol* 25: 1058–1072.
- 937 Nadachowska-Brzyska, K., C. Li, L. Smeds, G. Zhang, and H. Ellegren, 2015 Temporal
938 dynamics of avian populations during Pleistocene revealed by whole-genome sequences.
939 *Curr Biol* 25: 1375–1380.
- 940 Nei, M., T. Maruyama, and R. Chakraborty, 1975 The bottleneck effect and genetic variability in
941 populations. *Evolution* 29: 1–10.
- 942 Nelson, M. R., D. Wegmann, M. G. Ehm, D. Kessner, P. S. Jean *et al.*, 2012 An abundance of
943 rare functional variants in 202 drug target genes sequenced in 14,002 people. *Science* 337:
944 100–104.
- 945 Nielsen, R., 2000 Estimation of population parameters and recombination rates from single
946 nucleotide polymorphisms. *Genetics* 154: 931–942.
- 947 Nielsen, R., M. J. Hubisz, I. Hellmann, D. Torgerson, A. M. Andres *et al.*, 2009 Darwinian and
948 demographic forces affecting human protein coding genes. *Genome Res* 19: 838–849.
- 949 Nielsen, R., J. S. Paul, A. Albrechtsen, and Y. S. Song, 2011 Genotype and SNP calling from
950 next-generation sequencing data. *Nature Rev Genet* 12: 443–451.
- 951 Orlando, L., A. Ginolhac, G. Zhang, D. Froese, A. Albrechtsen *et al.*, 2013 Recalibrating *Equus*
952 evolution using the genome sequence of an early Middle Pleistocene horse. *Nature* 499: 74–
953 78.
- 954 Orozco-terWengel, P., 2016 The devil is in the details: the effect of population structure on
955 demographic inference. *Heredity* 116: 349–350.
- 956 Pagani, L., D. J. Lawson, E. Jagoda, A. Mörseburg, A. Eriksson *et al.*, 2016 Genomic analyses
957 inform on migration events during the peopling of Eurasia. *Nature* 538: 238–242.
- 958 Palkopoulou, E., S. Mallick, P. Skoglund, J. Enk, N. Rohland *et al.*, 2015 Complete genomes
959 reveal signatures of demographic and genetic declines in the woolly mammoth. *Curr Biol* 25:
960 1395–1400.
- 961 Peter, B. M., D. Wegmann, and L. Excoffier, 2010 Distinguishing between population bottleneck
962 and population subdivision by a Bayesian model choice procedure. *Mol Ecol* 19: 4648–4660.
- 963 Phung, T. N., C. D. Huber, and K. E. Lohmueller, 2016 Determining the effect of natural
964 selection on linked neutral divergence across species. *PLoS Genet* 12: e1006199.
- 965 Plagnol, V., and J. D. Wall, 2006 Possible ancestral structure in human populations. *PLoS Genet*
966 2: e105.
- 967 Polanski, A., and M. Kimmel, 2003 New explicit expressions for relative frequencies of single-

- 968 nucleotide polymorphisms with application to statistical inference on population growth.
969 *Genetics* 165: 427–436.
- 970 Prado-Martinez, J., P. H. Sudmant, J. M. Kidd, H. Li, J. L. Kelley *et al.*, 2013 Great ape genetic
971 diversity and population history. *Nature* 499: 471–475.
- 972 Prufer, K., F. Racimo, N. Patterson, F. Jay, S. Sankararaman *et al.*, 2014 The complete genome
973 sequence of a Neanderthal from the Altai Mountains. *Nature* 505: 43–49.
- 974 Ptak, S. E., and M. Przeworski, 2002 Evidence for population growth in humans is confounded
975 by fine-scale population structure. *Trends Genet* 18: 559–563.
- 976 Schiffels, S., and R. Durbin, 2014 Inferring human population size and separation history from
977 multiple genome sequences. *Nat Genet* 46: 919–925.
- 978 Scholz, C. A., T. C. Johnson, A. S. Cohen, J. W. King, J. A. Peck *et al.*, 2007 East African
979 megadroughts between 135 and 75 thousand years ago and bearing on early-modern human
980 origins. *Proc Natl Acad Sci USA* 104: 16416–16421.
- 981 Schraiber, J. G., and J. M. Akey, 2015 Methods and models for unravelling human evolutionary
982 history. *Nature Rev Genet* 16: 727.
- 983 Schrider, D. R., A. G. Shanku, and A. D. Kern, 2016 Effects of linked selective sweeps on
984 demographic inference and model selection. *Genetics* 204: 1207–1223.
- 985 Sjödin, P., A. E. Sjöstrand, M. Jakobsson, and M. G. Blum, 2012 Resequencing data provide no
986 evidence for a human bottleneck in Africa during the penultimate glacial period. *Mol Biol*
987 *Evol* 29: 1851–1860.
- 988 Slatkin, M., and R. R. Hudson, 1991 Pairwise comparisons of mitochondrial DNA sequences in
989 stable and exponentially growing populations. *Genetics* 129: 555–562.
- 990 Song, S., E. Sliwerska, S. Emery, and J. M. Kidd, 2016 Modeling human population separation
991 history using physically phased genomes. *Genetics* 205: 385–395.
- 992 Sovic, M. G., B. C. Carstens, and H. L. Gibbs, 2016 Genetic diversity in migratory bats: Results
993 from RADseq data for three tree bat species at an Ohio windfarm. *PeerJ* 4: e1647.
- 994 Tajima, F., 1989 The effect of change in population size on DNA polymorphism. *Genetics* 123:
995 597–601.
- 996 Takahata, N., and Y. Satta, 1998 Footprints of intragenic recombination at HLA loci.
997 *Immunogenetics* 47: 430–441.
- 998 Takahata, N., Y. Satta, and J. Klein, 1995 Divergence time and population size in the lineage
999 leading to modern humans. *Theor Popul Biol* 48: 198–221.

- 1000 Tennesen, J. A., A. W. Bigham, T. D. O'Connor, W. Fu, E. E. Kenny *et al.*, 2012 Evolution and
1001 functional impact of rare coding variation from deep sequencing of human exomes. *Science*
1002 337: 64–69.
- 1003 Terhorst, J., and Y. S. Song, 2015 Fundamental limits on the accuracy of demographic inference
1004 based on the sample frequency spectrum. *Proc Natl Acad Sci USA* 112: 7677–7682.
- 1005 Terhorst, J., J. A. Kamm, and Y. S. Song, 2017 Robust and scalable inference of population
1006 history from hundreds of unphased whole genomes. *Nat Genet* 49: 303–309.
- 1007 Thornton, K., and P. Andolfatto, 2006 Approximate Bayesian inference reveals evidence for a
1008 recent, severe bottleneck in a Netherlands population of *Drosophila melanogaster*. *Genetics*
1009 172: 1607–1619.
- 1010 Trucchi, E., P. Gratton, J. D. Whittington, R. Cristofari, Y. Le Maho *et al.*, 2014 King penguin
1011 demography since the last glaciation inferred from genome-wide data. *Proc R Soc Lond*
1012 [Biol] 281: 20140528.
- 1013 Wakeley, J., 2009 *Coalescent theory: an introduction*. Roberts & Co. Publishers., Greenwood
1014 Village.
- 1015 Wall, J. D., and J. K. Pritchard, 2003 Haplotype blocks and linkage disequilibrium in the human
1016 genome. *Nature Rev Genet* 4: 587.
- 1017 Wang, G.-D., W. Zhai, H.-C. Yang, L. Wang, L. Zhong *et al.*, 2016 Out of southern East Asia:
1018 the natural history of domestic dogs across the world. *Cell Res* 26: 21–33.
- 1019 Weissman, D. B., and O. Hallatschek, 2017 Minimal-assumption inference from population-
1020 genomic data. *eLife* 6:.
- 1021 Zhao, S., P. Zheng, S. Dong, X. Zhan, Q. Wu *et al.*, 2012 Whole-genome sequencing of giant
1022 pandas provides insights into demographic history and local adaptation. *Nat Genet* 45: 67–
1023 71.

1024 DATA ACCESSIBILITY

1025 All code to simulate data under each demographic model and calculate heterozygosity and
1026 generate the SFS from simulated and empirical data are available on GitHub:
1027 github.com/LohmuellerLab/Compare_Demographic_Models

1028

1029

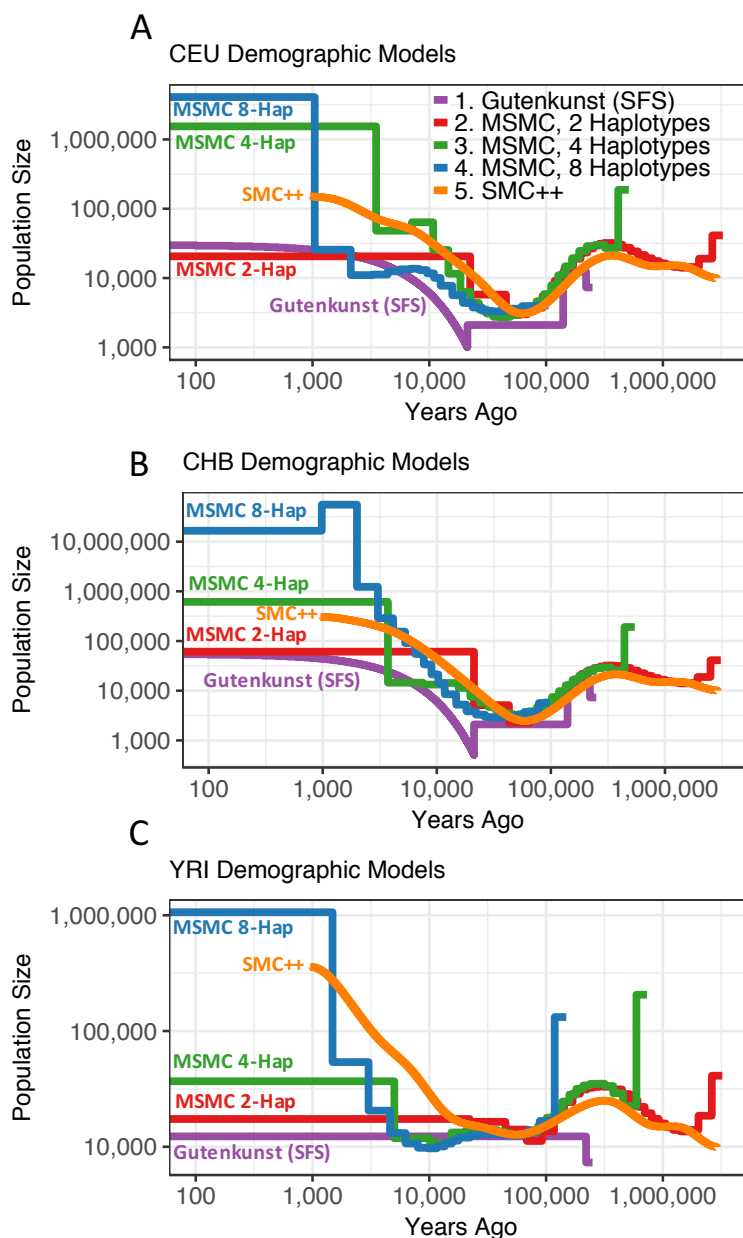
1030

AUTHOR CONTRIBUTIONS

1031 KEL and ACB conceived the study. ACB carried out all analyses based on the demographic
1032 models, and TNP carried out all empirical analyses based on the 1000 Genomes data. ACB
1033 generated all figures. ACB, TNP and KEL all participated in manuscript preparation.

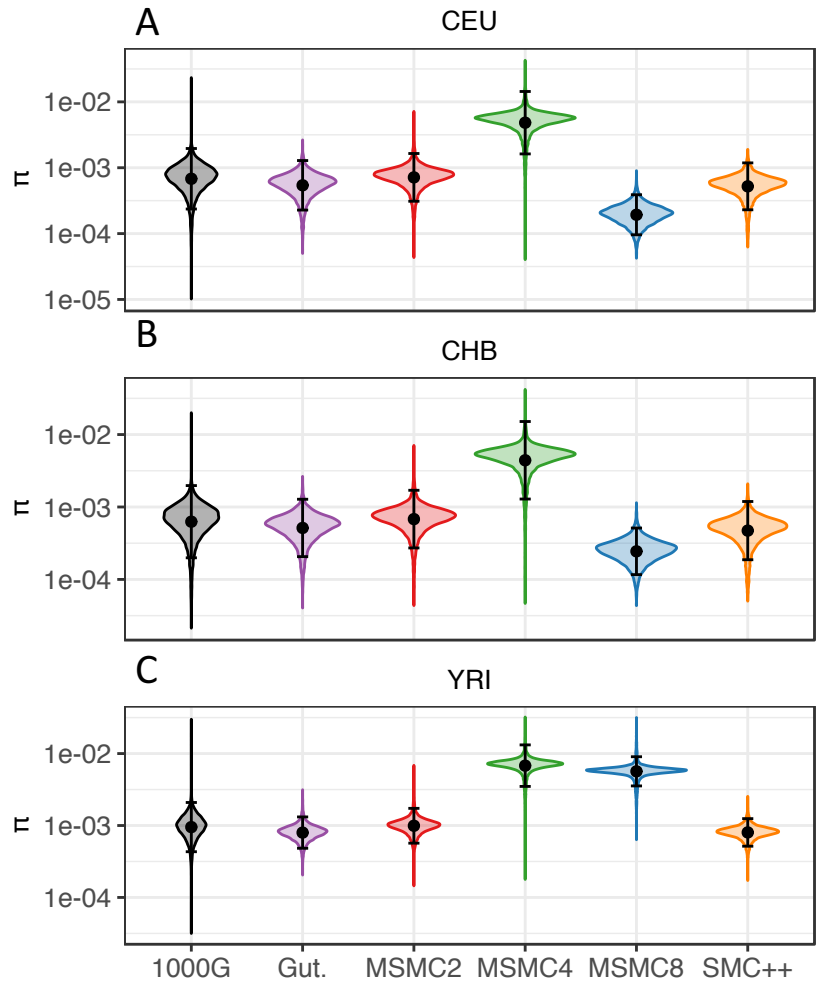
1034

1035



1037

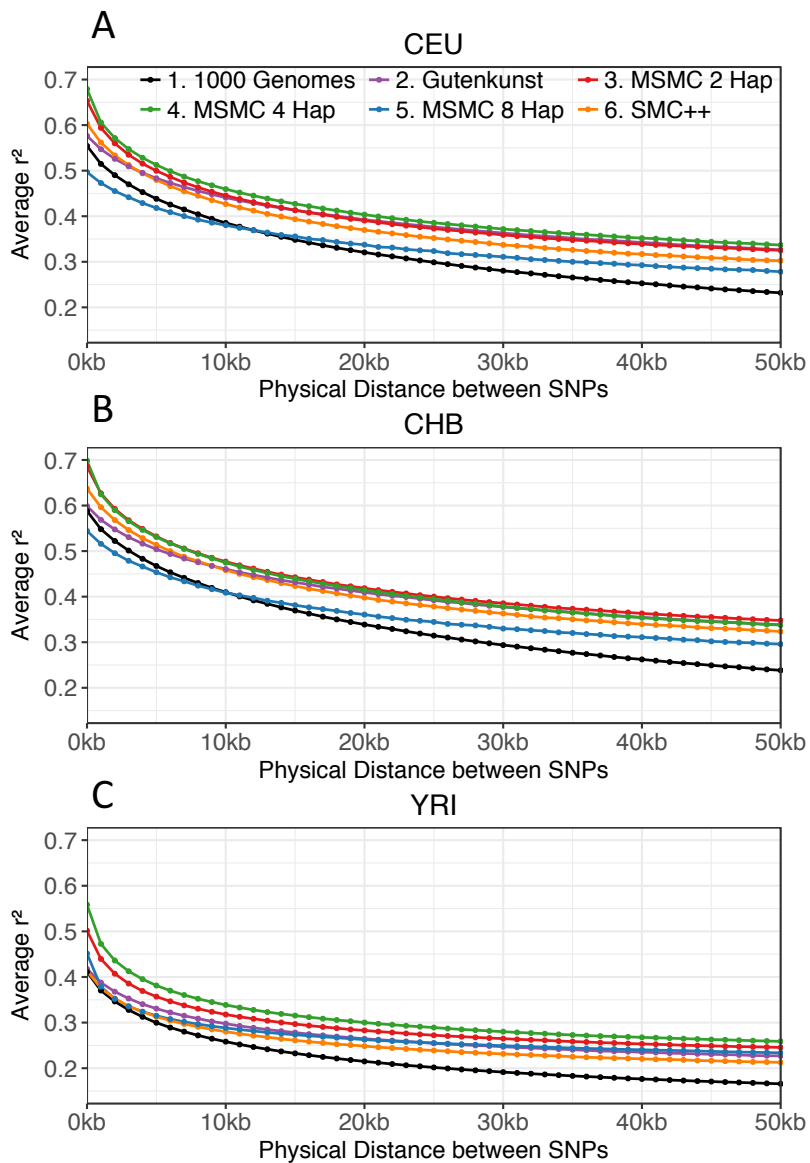
1038 **Figure 1. Demographic histories for the CEU (A), CHB (B), and YRI (C) populations.** Trajectories
 1039 are log-scaled and in terms of physical units (diploid individuals and years). Models were either inferred
 1040 using SFS-based methods (“Gutenkunst”) by Gutenkunst *et al.* (2009), from a sequentially Markovian
 1041 coalescent-based approach (“MSMC”) from two, four and eight haplotypes by Schiffels and Durbin
 1042 (2014), or using a combined SFS and whole genome approach (“SMC++”) by Terhorst *et al.* (2017). The
 1043 Gutenkunst models also include migration between all three populations, not depicted here. Models are
 1044 scaled by the generation times used in each study (Gutenkunst *et al.* (2009): 25 years/generation; Schiffels
 1045 and Durbin (2014): 30 years/generation; Terhorst *et al.* (2017): 29 years/generation).



1046

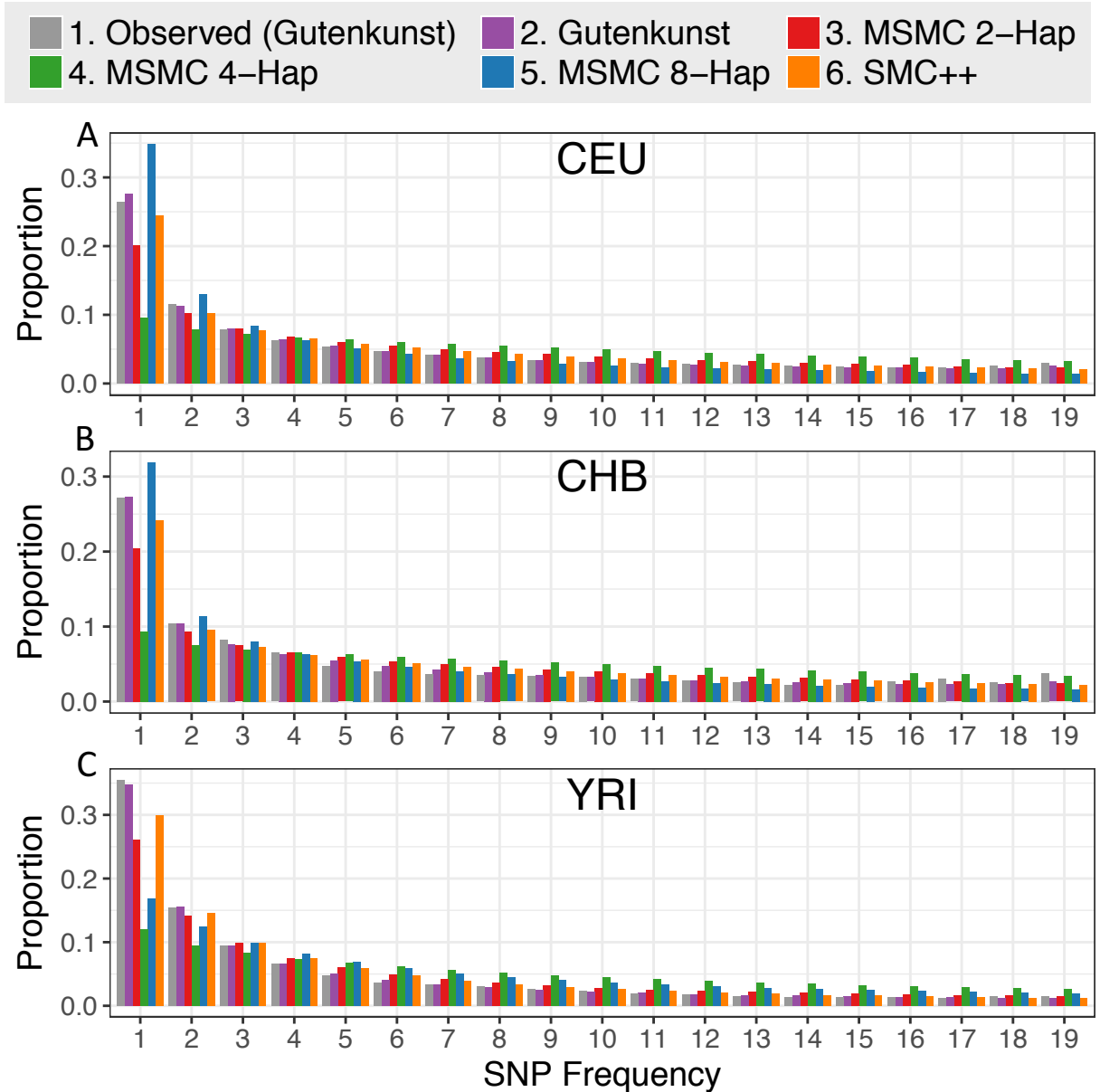
1047
 1048
 1049
 1050
 1051
 1052

Figure 2. Kernel density distribution of expected heterozygosity (π per site). Heterozygosity was calculated across 100kb windows from whole genome 1000 Genomes project data for CEU (A), CHB (B), and YRI (C), and from 20,000 x 100kb blocks for data simulated under each demographic model. The black dot and bars indicate the mean \pm two standard deviations for each distribution. Note the log-10 scaling on the y-axis.



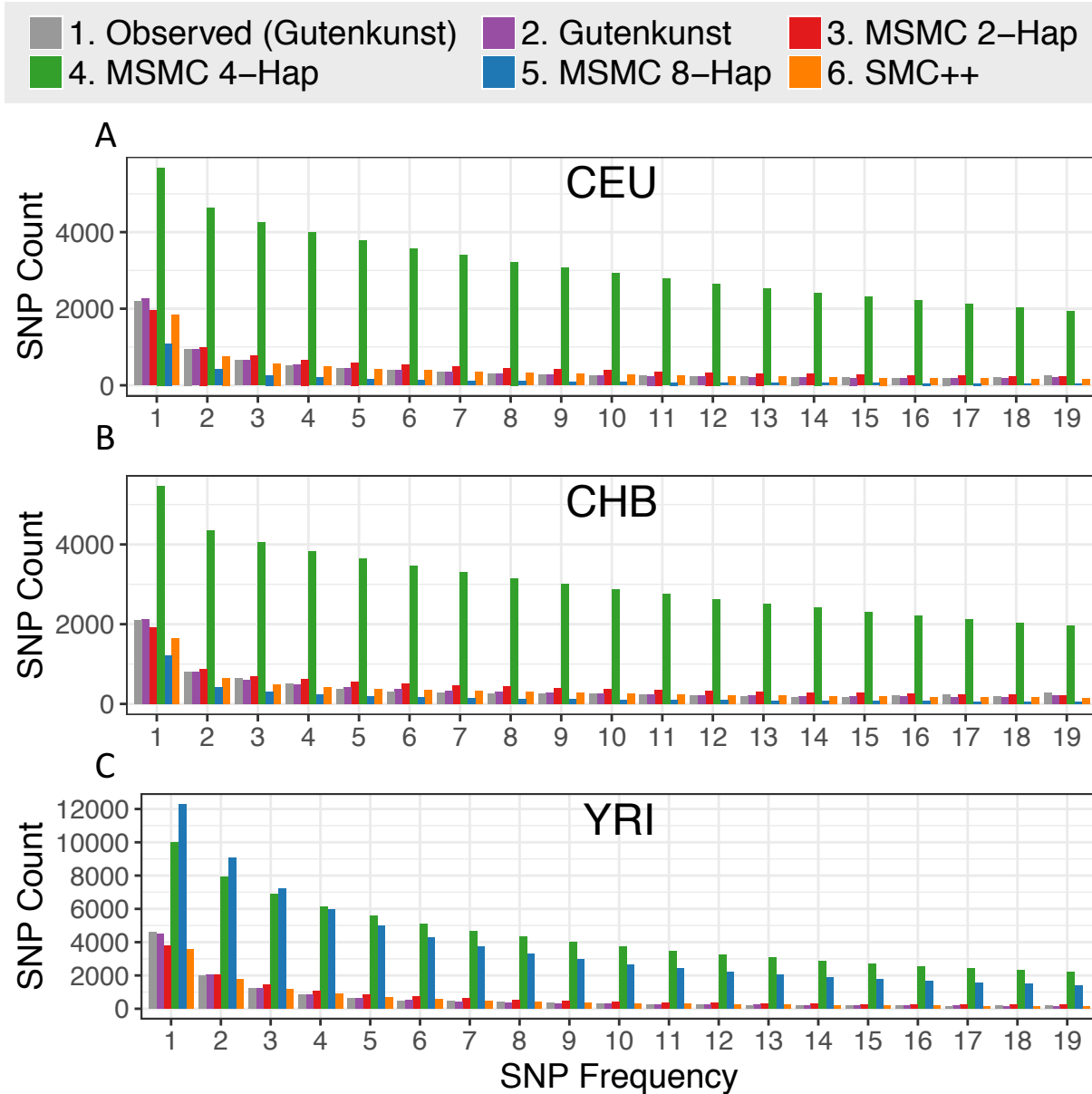
1053
 1054
 1055
 1056
 1057
 1058
 1059

Figure 3. Linkage disequilibrium (LD) decay patterns. LD decay was calculated across 100kb windows from 1000 Genomes data and simulated data under each demographic model for CEU (A), CHB (B), and YRI (C). Pairs of SNPs are binned based on physical distance (bp) between them, up to 51kb. Average genotype r^2 is calculated within each distance bin.



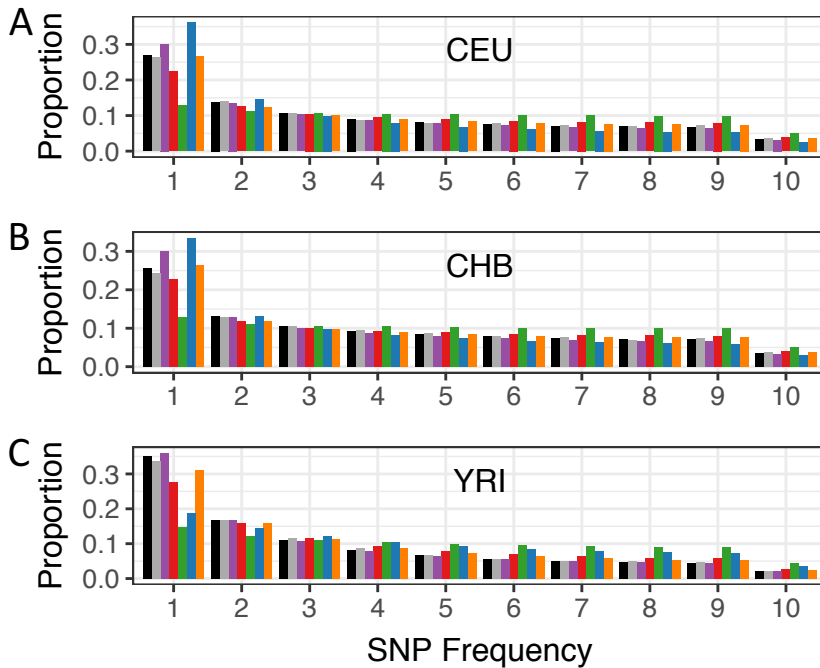
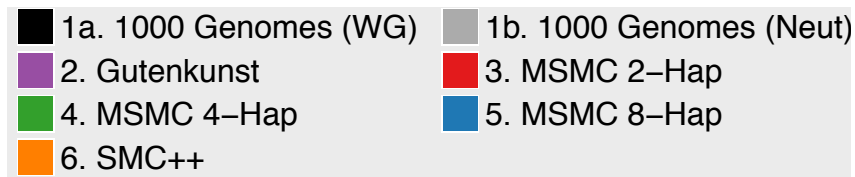
1060
 1061
 1062
 1063
 1064
 1065
 1066

Figure 4. Unfolded proportional site frequency spectra for CEU (A), CHB (B), and YRI (C) populations. The “Observed” SFS is from noncoding sequence used by Gutenkunst *et al.* (2009) to infer demographic histories for these three populations. See **Figure S5** for scaling using alternative mutation rates.



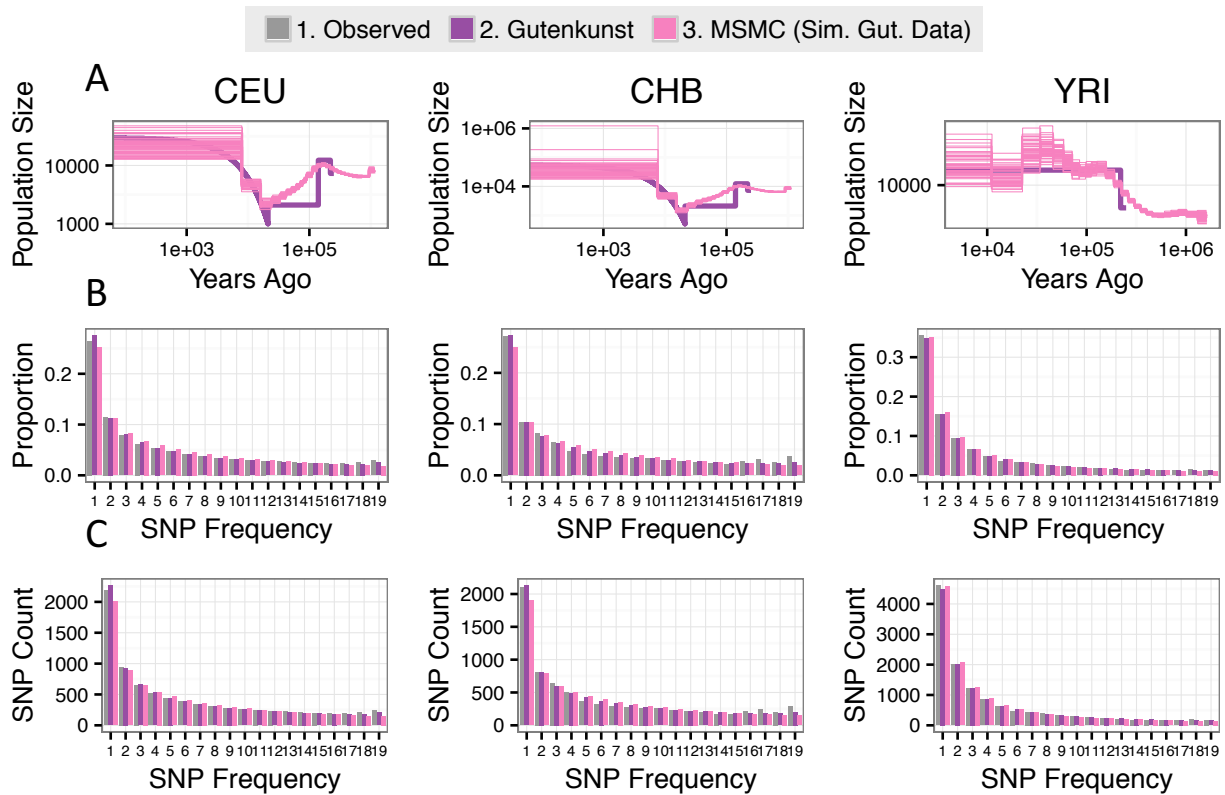
1067
 1068
 1069
 1070
 1071
 1072
 1073
 1074
 1075

Figure 5. SNP count site frequency spectra using the counts of SNPs for the CEU (A), CHB (B), and YRI (C) populations. The “Observed” SFS is from noncoding sequence used by Gutenkunst *et al.* (2009) to infer demographic histories for these three populations. SFSs are scaled using the ancestral population size given by each model, the mutation rate used to scale each model by the authors and the sequence length of the empirical dataset (4.04Mb). See **Figure S6** for scaling using alternative mutation rates.



1076
1077
1078
1079
1080
1081

Figure 6. Folded proportional site frequency spectra for CEU (A), CHB (B), and YRI (C) populations. The “1000 Genomes (WG)” SFS is from low-coverage whole genome 1000 Genomes data, and the “1000 Genomes (Neut)” SFS is from 6333 x 10kb putatively neutral regions in the 1000 Genomes data.



1082
 1083
 1084
 1085
 1086
 1087
 1088
 1089
 1090
 1091
 1092
 1093
 1094
 1095

Figure 7. MSMC 2-Haplotype can accurately infer the demographic model predicted by Gutenkunst *et al.* (2009). (A) shows the results of running MSMC 2-Haplotype on 50 independent 2-haplotype datasets simulated under the Gutenkunst *et al.* (2009) model of human demographic history (“Gutenkunst,” heavy purple line). The resulting MSMC 2-Haplotype trajectories (“MSMC Sim. Gut. Data,” fine pink lines) show the MSMC trajectories inferred from these 50 datasets. Note that these trajectories accurately track the demographic model used to simulate the data. (B) and (C) show proportional and SNP count site frequency spectra for each population, respectively. The gray bars (Observed) denote the empirical SFS used by Gutenkunst *et al.* (2009). The purple bars denote the expected SFS under the inferred Gutenkunst demographic models. The pink bars denote the expected SFS under the average of the 50 MSMC 2-Haplotype demographic model trajectories for each population. Note that these three SFSs agree.